Selective labeling of single-walled carbon nanotubes using solid binding proteins

Sonja June Glaser Dunakey

A thesis

Submitted in partial fulfillment of the

Requirements for the degree of

Master of Science

University of Washington

2018

Committee:

François Baneyx (Chair)

David Castner

Program Authorized to Offer Degree:

Department of Chemical Engineering

University of Washington

Abstract

Selective Labeling of single-walled carbon nanotubes using solid binding proteins

Sonja June Glaser Dunakey

Chair of the Supervisory Committee:
François Baneyx
Department of Chemical Engineering

Robust and simple strategies to noncovalently functionalize single walled carbon nanotubes (SWNT) are of considerable interest for building hybrid nanomaterials and biosensors. Here, we show that fusion of the Car9 and Car15 carbon binding peptides to the C-termini of the sfGFP and mCherry fluorescent protein scaffolds, allows for selective labeling of the ends and sidewalls of SWNT, respectively. By further modifying carbon-binding sfGFP derivatives through the engineering of a gold-binding peptide or a single cysteine residue in a solvent exposed loop that lies opposite to the carbon binding extensions, we further show that it is possible to produce dual material binders supporting the selective conjugation of Au nanoparticles to the ends and sidewalls of nanotubes. The approach described here is generic and should prove useful for controlled and hierarchical assembly of other hybrid materials. It also holds promise for the creation of reconfigurable assemblies through the use of stimuli-responsive protein scaffolds.

Introduction

Carbon nanotubes (CNTs) were discovered in 1991[1] and are best described as rolled up sheets of graphene – a lattice of sp^2-hybridized carbon. While graphene is a 2D metallic substance with ballistic conductance,[2] CNTs can exist either as single-walled (SWNT) or multi-walled (MWNT) structures, and exhibit metallic or semiconducting electronic properties, depending on how the hexagonal carbon lattice aligns with the nanotube axis or chiral vector.[3, 4] With extraordinary mechanical properties (a tensile strength up to 10 times that of stainless steel)[5] and an electrical conductivity up to 1000 times greater than that of copper,[6, 7] CNT have attracted much attention for application in composite materials.[8, 9] Additionally, semiconducting CNTs are of special interest for use in new types of biosensors.[10-12] As the conductivity of semiconducting CNTs is highly sensitive to their environment, their response is fast, and the detection area is scalable to the size of individual proteins.[13-15] However, CNT are notoriously difficult to disperse in aqueous solution due to their highly hydrophobic nature, and propensity to bundle and form insoluble aggregates.[16]

In order to overcome this issue, CNTs have often been treated with acids (e.g., HNO_3, H_2SO_4 and/or H_2O_2) to oxidize the carbon lattice and form reactive hydroxyl and carboxyl surface groups that both enhance solubility in polar solvents, and provide chemical "handles" for covalent conjugation of proteins and other species.[17] Unfortunately, this treatment also degrades the overall electrical properties that make CNT unique.[18] As a result, non-covalent approaches are preferred for CNT biofunctionalization. The simplest of these, non-specific adsorption, has significant limitations including lack of control of protein orientation, and the propensity for proteins to misfold and lose activity at the hydrophobic surface of CNT.[13, 19, 20] Amphiphilic polymers, such as polyethylene glycol modified with pyrene groups[17] and polystyrene modified with poly-acrylic acid[21], and surfactants such as such as sodium cholate, sodium dodecyl sulfate, and Triton,[17, 22-25] have also been used to coat the side walls of CNTs. Here, hydrophobic moieties bind nonspecifically to the tubes' walls (often wrapping around the entire structure)[21] while hydrophilic regions support their dispersion in aqueous solvents and provide an opportunity for protein conjugation through the introduction of NHS or maleimide groups.[24, 26, 27] However, the approach does not provide effective orientation control in the case of NHS chemistry, and requires the introduction of cysteine residues at specified location in the target in the case of maleimide chemistry. Attempts at controlling spatial specificity (e.g., end or wall binding) have also been made, but have involved oxidizing the nanotubes and using NHS coupling chemistry to covalently link a fluorophore to the ends of a CNT wrapped with Tween 20.[28] Finally, it is worth noting that none of the approaches discussed above provide a straightforward path for the creation of multicomponent hierarchical architectures.

Solid binding peptides (SBP) are short polypeptides typically identified by combinatorial phage or cell surface display for their ability to bind to inorganic materials.[29] SBPs have been selected against a broad range of substrates including carbon.[30-34] These carbon-binding peptides have been used in a synthetic form to resuspend and manipulate single and multiwalled CNTs and for building CNT-based nanostructures. For instance, Inoue et al. have used hetero-functional polypeptide scaffolds for precipitating titanium dioxide on SWNT,[35] Pender et al. have used hetero-functional polypeptides to sheathe SWNT in either silica or titanium dioxide,[33] and Kurppa et al. have used a hetero-functional polypeptide to form thin films of SWNT with gold

nanoparticles evenly spaced along their lengths.[20] These nanoarchitectures represent a fraction of the possibilities of building heterogeneous structures with SWNT, but have the similar issue as discussed above for polymer or surfactant functionalization of SWNT, of wrapping or completely coating the nanotube. By contrast, one or more SBPs can be genetically engineered within protein scaffolds to produce solid-binding proteins which combine the structural and/or functional properties of the scaffold with the adhesive or morphogenetic properties of the inserted SBP(s).[36]

In a previous study, Coyle et *al*.[37] reported on the isolation of SBPs exhibiting high affinity for evaporated carbon. Two of these, Car9 (DSARGFKKPGKR) and Car15 (RTYLPLPWMAAL) were selected for further characterization on the basis of their very different amino acid compositions: Car9 is highly basic and rather hydrophilic, while Car 15 is hydrophobic and contains a single positively charged residue. The two SBPs were found to exhibit distinct carbon-binding modalities by SPR, AFM, solubilization, and pull-down experiments, with Car15 preferentially binding to *sp*2- over *sp*3-hybridized carbon, and Car9 favoring the carbonyl, carboxyl and hydroxyl-rich edges of highly-oriented pyrolytic graphite (HOPG) and glassy carbon.[37] Consistent with these observations, Car9 was later found to bind to silanol-rich silica surfaces, enabling oriented immobilization,[38] controlled loading release,[39] and purification[40, 41] of Car9-tagged fusion proteins using inexpensive silica substrates. Because the side-walls of CNTs primarily consist of *sp*2-hybridized carbon, while their ends is *sp*3-like with significant defects in the carbon lattice and numerous free hydroxyl and carboxyl groups,[17] we set out to explore the use of Car15- and Car9 for the selective conjugation of proteins to CNT ends and edges. Here, we report on the design and use of Car9- and Car15-based fluorescent carbon-binding proteins to achieve selective, noncovalent modification of the ends and side walls of SWNT. We further show that derivatives of these proteins can be used to orchestrate the formation of hybrid nanostructures in which gold nanoparticles are coupled to nanotubes' walls or termini.

Results and Discussion

Selective labeling of the side wall and ends of carbon nanotubes from the powder state

To build easily detectable carbon binding proteins, we genetically fused the Car15 and Car9 sequences to the C-termini of the green fluorescent protein sfGFP (λ_{max}^{Ex} = 485 nm; λ_{max}^{Em} = 510 nm)[42] and the red fluorescent protein His-mCherry (λ_{max}^{Ex} = 587 nm; λ_{max}^{Em} = 610 nm).[43] These two fluorescent proteins fold into a similar β-barrel structure but share little sequence identity and are evolutionary unrelated (Fig. S1; sfGFP is a brighter and thermodynamically stable variant of *A. Victoria* GFP,[42] while His-mCherry is a monomeric and photostable variant of the *Dicosoma* DsRed protein[43] with a 6x-histidine tag on the N-terminus). A flexible GGGS linker was inserted between solid binding sequences and C-termini to allow each

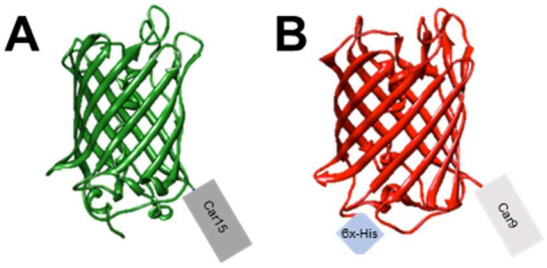

Figure 1: Schematic structure of (A) sfGFP-Car15 and (B) His-mCherry-Car9. The Car15 and Car9 CBP are represented by the dark gray and light gray squares respectively. The 6x-His tag is represented by the blue square

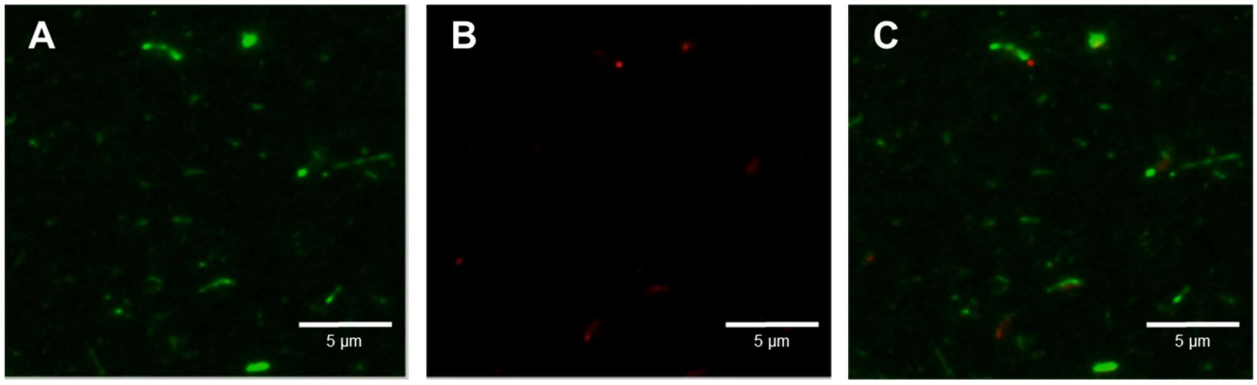

Figure 2: Fluorescence microscopy images (90x mag) of SWNT from dry powder after resuspension with sfGFP-Car15 and subsequent addition of His-mCherry-Car9 (A) excitation λ = 473 nm (B) excitation λ = 587 nm (C) overlay of (A) and (B). Average length (from Sigma) ~ 5 µm

SBP more degrees of freedom for carbon binding. The resulting proteins were named sfGFP-Car15 and His-mCherry-Car9 (Fig. 1).

In a first approach to test the ability of sfGFP-Car15 and His-mCherry-Car9 to support the solubilization of CNTs, we made use of single walled nanotubes (SWNT) obtained in a dry powder form from Sigma Aldrich. Initial experiments were conducted by directly dispersing SWNT with the fusion proteins incorporating Car9 and Car15. Briefly, SWNT (1 mg/mL) were taken into 50 mM phosphate buffer and sonicated in the presence of 1 µM of sfGFP-Car15 with subsequent addition of 0.5 µM of His-mCherry-Car9, as described in Materials and Methods. Examination of the samples by fluorescence microscopy under 480 nm excitation revealed the labeling of elongated objects by sfGFP-Car15 (Fig. 2A). We take these to be SWNT. A small number of discrete spots were also observed under illumination at 520 nm (Fig. 2B). Some of this punctuated red fluorescence connected to the zones of sfGFP-Car15 labeling in merged images (Fig. 2C), indicating that His-mCherry-Car9 occasionally binds to the ends of SWNT. Thus, the Car15 and Car9 SPBs appear suitable for providing selective recognition of the ends and side-walls of SWNT. However, although the sonication time was minimized so that colloidal suspensions sfGFP-Car15-solubilized CNTs were able to withstand centrifugation without bundling and precipitating, the sonication treatment still fractured and shortened nanotubes as previously reported,[8, 44] and as shown in supplementary Fig. S2. We therefore did not pursue further optimization of the sonication process but instead turned our attention to a more gentle approach based on dialysis.

Selective labeling of the side wall and ends of carbon nanotubes by surfactant exchange

Surfactants, both charged, such as sodium cholate and sodium dodecyl sulfate, and neutral, such as Triton, have long been used to improve the dispersion of carbon nanotubes in aqueous solvents.[17, 22-24] To determine if efficient end- and side wall-labeling of SWNT could be achieved by replacing surfactant molecules with carbon-binding proteins, we purchased semiconducting SWNT (metallic SWNT functionalization shown in supplementary Fig. S3) replaced the proprietary detergent used for their stabilization by sodium cholate, and conducted extensive dialysis experiments in the presence of Car9 and Car15-tagged proteins.

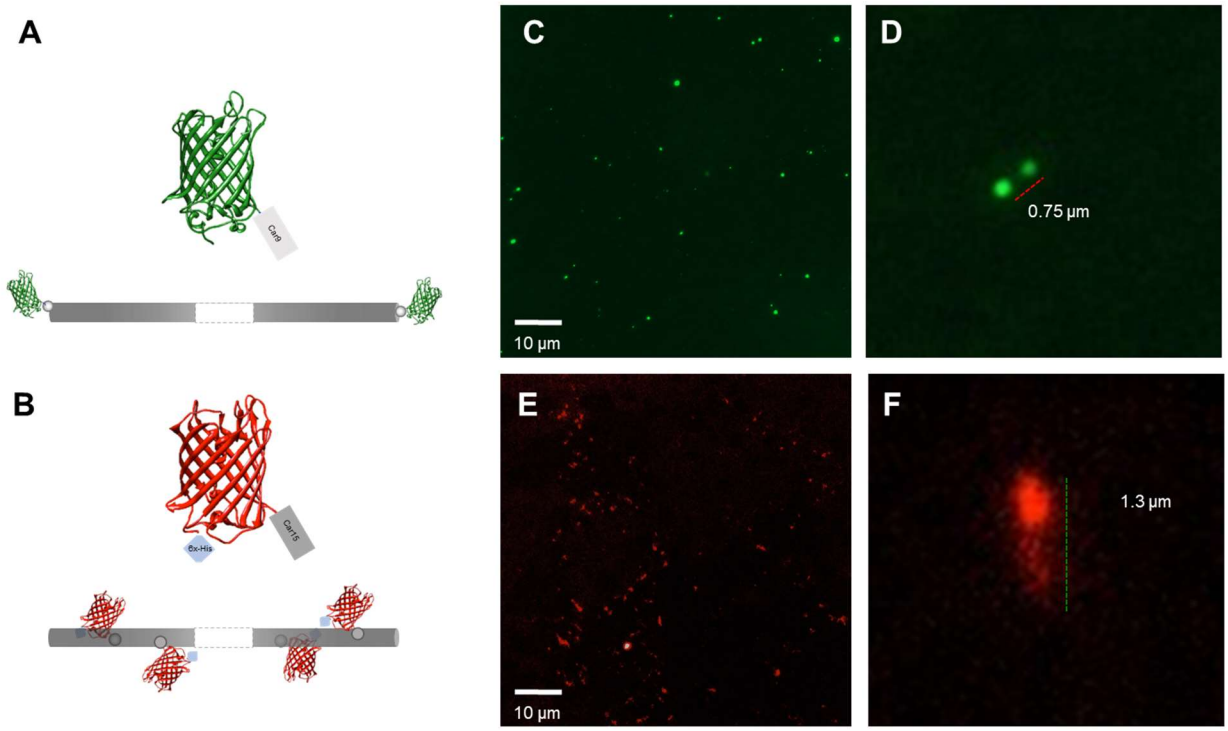

Figure 3: Fluorescence microscopy images (90x mag) of SWNT after suspension through surfactant exchange with sfGFP-Car9 or His-mCherry-Car15. (A) Schematic of sfGFP-Car9 binding to ends of SWNT. (B) Schematic of His-mCherry-Car15 binding to walls of SWNT. (C) Wide-view of SWNT labeled with sfGFP-Car9 excitation λ = 473 nm. (D) Zoom in of single feature from B showing fluorescent labeling of SWNT on ends by sfGFP-Car9. (E) Wide-view of SWNT labeled with His-mCherry-Car15 excitation λ = 587 nm. (F) Zoom of single feature from E showing fluorescent labeling of SWNT along length by His-mCherry-Car15.

Rather than using His-mCherry-Car9 and sfGFP-Car15, as in the experiment of Fig. 1, we employed two swapped constructs – His-mCherry-Car15 and sfGFP-Car9 (Fig. 3A and 3B) – because they allowed for the removal of unbound proteins remaining in solution at the conclusion of the ligand exchange step by orthogonal affinity purification techniques (Ni-NTA chromatography for His-mCherry-Car15[45] and silica chromatography for sfGFP-Car9[40]). This feature not only improved the quality of fluorescence images by removing the significant background fluorescence contributed by free proteins, but also enabled sequential labeling and decoration schemes (see below). Suspensions of sfGFP-Car9- and His-mCherry-Car15-decorated SWNT were stable for up to 8 weeks. However, removal of excess protein by affinity chromatography led to a reduction in stability, with aggregates starting to precipitate within 10 days.

The dialysis-based ligand exchange strategy resulted in fluorescence fields exhibiting punctuated features in the case of sfGFP-Car9 or more extended ones in the case of His-mCherry-Car15 (Fig. 3), consistent with these proteins binding to the ends and side walls of SWNT, respectively. In the case of sfGFP-Car9, fluorescent spots often appeared to be paired, with separation distance in sparsely populated fields consistent with typical nanotube lengths once the diffraction limit is taken into account (Fig. 3C and 3D, supplementary Fig. S4). By contrast, magnified images of His-mCherry-Car15-supplemented SWNT revealed clustered fluorescence with a high aspect ratio, as

would be expected upon side-wall labeling (Fig. 3E and 3F). These results confirm the selectivity of the Car9 and Car15 SBPs for the ends and walls of SWNTs and confirm the suitability of dialysis-based ligand exchange for the noncovalent coupling of solubilizing solid-binding proteins to carbon nanostructures.

Hetero-bifunctional solid binding proteins for SWNT- and gold-binding

One of the advantages of solid binding proteins relative to synthetic SBPs is that their framework can be genetically engineered to display two or more inorganic-binding sequences at spatial locations, and with orientations that are fully defined by the structure of the host scaffold.[36] Having previously showed that it was possible to display two functional SBPs at the C-terminus and within loop9 of sfGFP, two positions that lie on opposite sides of the protein's β-barrel,[46] we set out to exploit the permissive loop 9 location[42] to endow sfGFP-Car9 and sfGFP-Car15 with gold-binding functionality. The choice of gold was motivated by the unique plasmonic properties of gold nanoparticles,[47] and the possibility of using dual carbon/gold binding proteins to direct nanotubes to gold contacts for the fabrication of SWNT-based transistors.[13, 21, 24, 27]. We also chose to compare a gold-binding SBP to the well known ability of cysteine residues to coordinate gold,[48] as protein binding to gold has been reported to be influenced by surface curvature.[49] Thus, we engineered the Ag4 gold-binding peptide (NPSSLFRYLPSD)[50] into loop 9 of sfGFP-Car9[46] and used site-directed mutagenesis to introduce the Cys48-Ser and Gly51-Cys mutations in loop 3 of sfGFP, an additional permissive loop[42] opposite the β-barrel from the C-terminus (Supplementary Fig. S5 and S6, purified proteins shown in Supplementary Fig. S7).

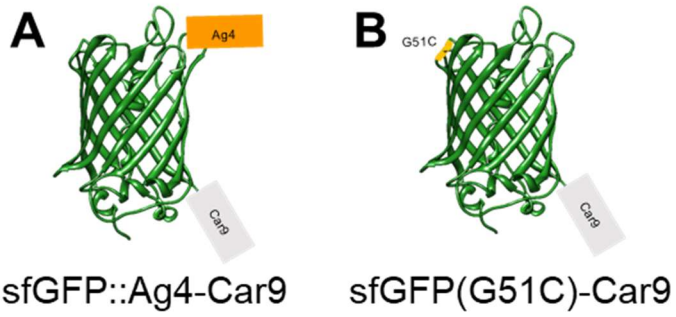

Figure 4: Schematic structure of (A) sfGFP::Ag4-Car9 and (B) sfGFP(G51C)-Car9. The Ag4 and Car9 SBPs are depicted as orange and light gray squares, respectively. The C48S/G51C mutation is depicted as a yellow line in the ribbon structure.

To demonstrate that the resulting proteins – sfGFP::Ag4-Car9 and sfGFP(G51C)-Car9 (Fig. 4A and 4B) – combine gold- and SWNT-end binding abilities, we first mixed purified polypeptides with citrate-stabilized Au nanoparticles 5 or 50 nm in diameter. Binding was assessed by measuring the shift of the gold surface plasmon resonance (SPR) peak which is modulated by nanoparticle size, the identity and surface coverage of bound ligands, and surrounding environment.[51, 52] For example, the SPR of 12 nm gold nanoparticles red shifts by ~2 nm upon conjugation of PEG molecules which affect the local refractive index around the particles.[53] Fig. 5 and Table 1 show that the maximum absorption wavelength of Au nanoparticles also changed by ~2 nm following incubation with 0.5 μM of wild type sfGFP. We attribute this shift to nonspecific binding, as a similar effect has been observed for the binding of bovine serum albumin (BSA), myoglobin, and cytochrome *c* to gold nanoparticles, both undecorated[49, 54, 55] and decorated with thiolated, methoxy-terminated PEG[56] or mercaptoundecanoic acid.[57] More surprisingly, we observed an about 6 nm red shift in the SPR peak of 5 and 50 nm Au particles upon addition of sfGFP-Car9, suggesting that the Car9 extension

confers the sfGFP framework additional affinity for gold. Remarkably, this value was comparable to that observed when Au nanoparticles were mixed with the gold-specific sfGFP::Ag4-Car9 variant (Fig. 5, traces red and yellow). However, it was the cysteine-containing sfGFP(G51C)-Car9 construct that induced the largest change (~9 nm) in the SPR peak of 5 nm Au nanoparticles, suggesting that Cys-51 has higher affinity for gold than the loop 9-displayed Ag4 SBP. In the case of 50 nm Au nanoparticles, the plasmon peak increased by 46 nm and the spectrum broadened indicating the production of a broad distribution of aggregated particles.[53, 58, 59] This behavior likely originates from the binding of multiple sfGFP(G51C)-Car9 molecules to the surface of large Au nanoparticles through high-affinity Cys-51 contacts, and their subsequent aggregation driven by lower affinity Car9 contacts (Supplementary Fig. S8) . Why the same phenomenon is not observed with sfGFP::Ag4-Car9 remains unclear but may be related to the fact that Ag4 has a lower affinity for 50 nm Au nanoparticles than the thiol group of Cys-51.

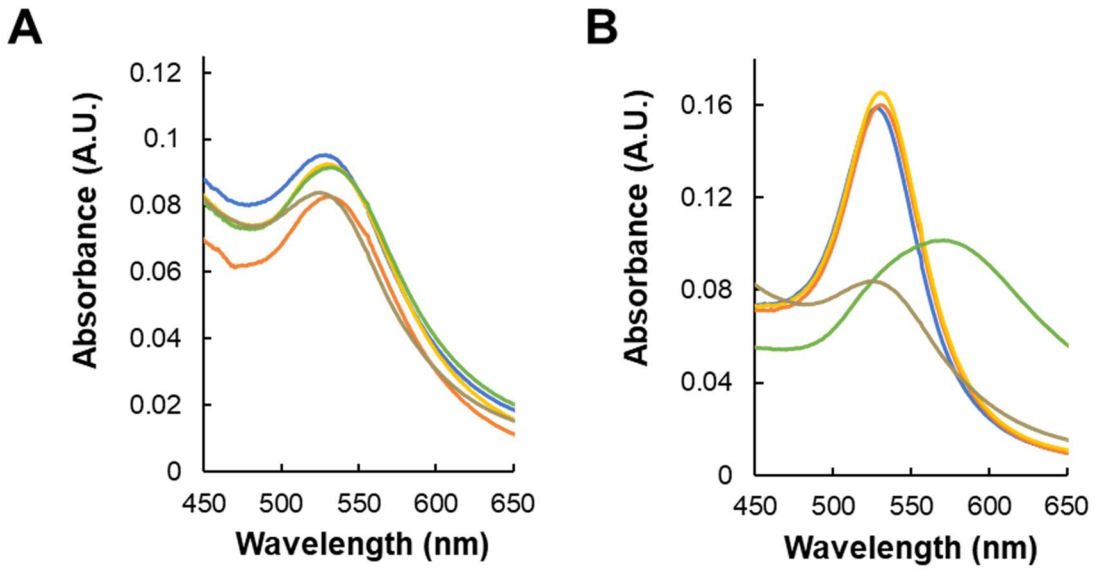

Figure 5: (A) Absorbance spectra of Au (5 nm) + protein [no additive (brown), sfGFP (blue), sfGFP-Car9 (red), sfGFP::Ag4-Car9 (yellow), sfGFP(G51C)-Car9 (green)] solutions showing gold surface plasmon resonance (SPR) peak. (B) Absorbance spectra of Au (50 nm) + protein [same colors as (A)] solutions showing gold SPR peak.

Au NP Size	5 nm		50 nm	
	SPR Peak	SPR Peak Shift	SPR Peak	SPR Peak Shift
Pure Au NP	525	-	525	-
sfGFP	527	+2	527	+2
sfGFP-Car9	531	+6	531	+6
sfGFP::Ag4-Car9	531	+6	531	+6
sfGFP(G51C)-Car9	534	+9	571	+46

Table 1: Tabulated values of SPR maximum for each Au + protein solution and their SPR peak shift relative to pure Au nanoparticles.

To confirm that the shift in the plasmon band of colloidal gold observed in the presence of sfGFP::Ag4-Car9 and sfGFP(G51C)-Car9 resulted from the binding of the Ag4 SBP or the Cys-51 thiol to the nanoparticle surface, we first adsorbed the proteins to silica to sequester the Car9 extension and preclude nonspecific binding. As expected, all fluorescent material partitioned with the silica, indicating quantitative binding of the Car9 extension to the solid phase (Fig. 6A). Next, 50 nm gold nanoparticles (or 5 nm particles, Fig. S9) were added to the mixture and the UV-visible spectra of the supernatants were recorded (Fig. 6C). Quantification of maximum intensities at 525 nm revealed that about 20% of the supplied gold nanoparticles bound nonspecifically to sfGFP-Car9 immobilized on silica. By contrast, immobilized sfGFP::Ag4-Car9 and sfGFP(G51C)-Car9 were capable of capturing about 40% and 70% of the nanoparticles, respectively (Fig. 6D). High affinity binding of 50 nm Au nanoparticles by immobilized sfGFP(G51C)-Car9 could be visually confirmed by the pink appearance of the silica phase under white light illumination (Fig. 6B). We conclude that both the silica/carbon and gold-binding activities of sfGFP::Ag4-Car9 and sfGFP(G51C)-Car9 are functional. Because, Au binding was more efficient in the case of sfGFP(G51C)-Car9, we selected this protein for subsequent experiments.

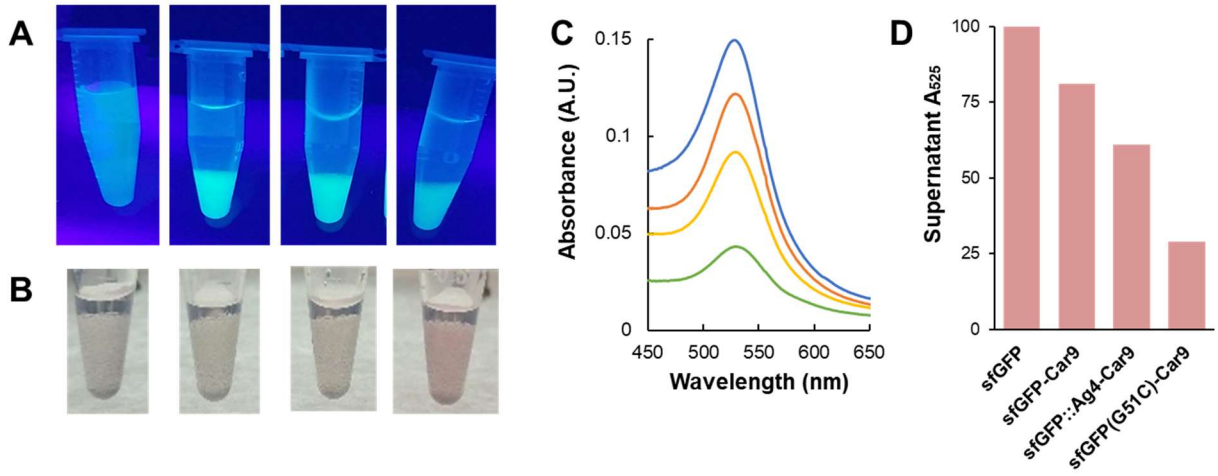

Figure 6: (A) sfGFP variants mixed with silica beads and photographed under 365 nm light [left to right sfGFP, sfGFP-Car9, sfGFP::Ag4-Car9, sfGFP(G51C)-Car9]. (B) Silica beads after protein and Au (50 nm) incubation. (C) Absorbance spectra of supernatants from B [sfGFP (blue), sfGFP-Car9 (red), sfGFP::Ag4-Car9 (yellow), sfGFP(G51C)-Car9 (green)]. (D) Percent Au (50 nm) remaining in supernatant after incubation with protein and silica as measured by absorbance at 525 nm.

Building SWNT/Au nanostructures using selective affinity of Car9 and Car15

With sfGFP(G51C)-Car9 in hand, we constructed a companion His-sfGFP(G51C)-Car15 (Supplementary Fig. S10, Fig. S11) solid-binding protein combining the SWNT side wall-binding activity of His-mCherry-Car15 with the gold-binding ability of sfGFP(G51C)-Car9. Bifunctionality was tested utilizing the 6x-His tag and the Cys51 in a similar pull-down experiment as for sfGFP(G51C)-Car9 (Supplementary Fig. S12). We next set out to demonstrate that the two proteins were suitable for controlled assembly of Au nanoparticles onto SWNT templates using 50 nm nanoparticles for ease of SEM imaging. Because both polyhistidine extensions[60] and Car9 (Fig. 5) exhibit some degree of affinity for gold, order of addition was important. Accordingly, we

first noncovalently adsorbed proteins to SWNT using the ligand exchange strategy of Fig. 3, and incubated the conjugates with gold nanoparticles before imaging samples by SEM.

Consistent with the fluorescent microscopy data of Fig. 3C, Au nanoparticles were found in pairs and separated by distances that averaged 600 nm in the case of sfGFP(G51C)-Car9-treated SWNT (Fig. 7C; also see supplementary Fig. S13). By contrast, particles were often found in linear groupings of more than two, and with separation distances averaging 180 nm, in SWNT samples derivatized with His-sfGFP(G51C)-Car15 (Fig. 7D; also see supplementary Fig. S14). Both behaviors were in sharp contrast with the random distribution and large separation distances (>2 μm) observed in the case of unconjugated gold nanoparticles (Fig. 7B). We conclude that sfGFP frameworks engineered with SBPs that specifically recognize the side walls (Car15) or ends (Car9) of SWNT, along with oppositely-located gold-binding functionalities (in this case Cys residue located in loop 3 of sfGFP), are suitable to orchestrate the organization of gold nanoparticles on nanotube templates.

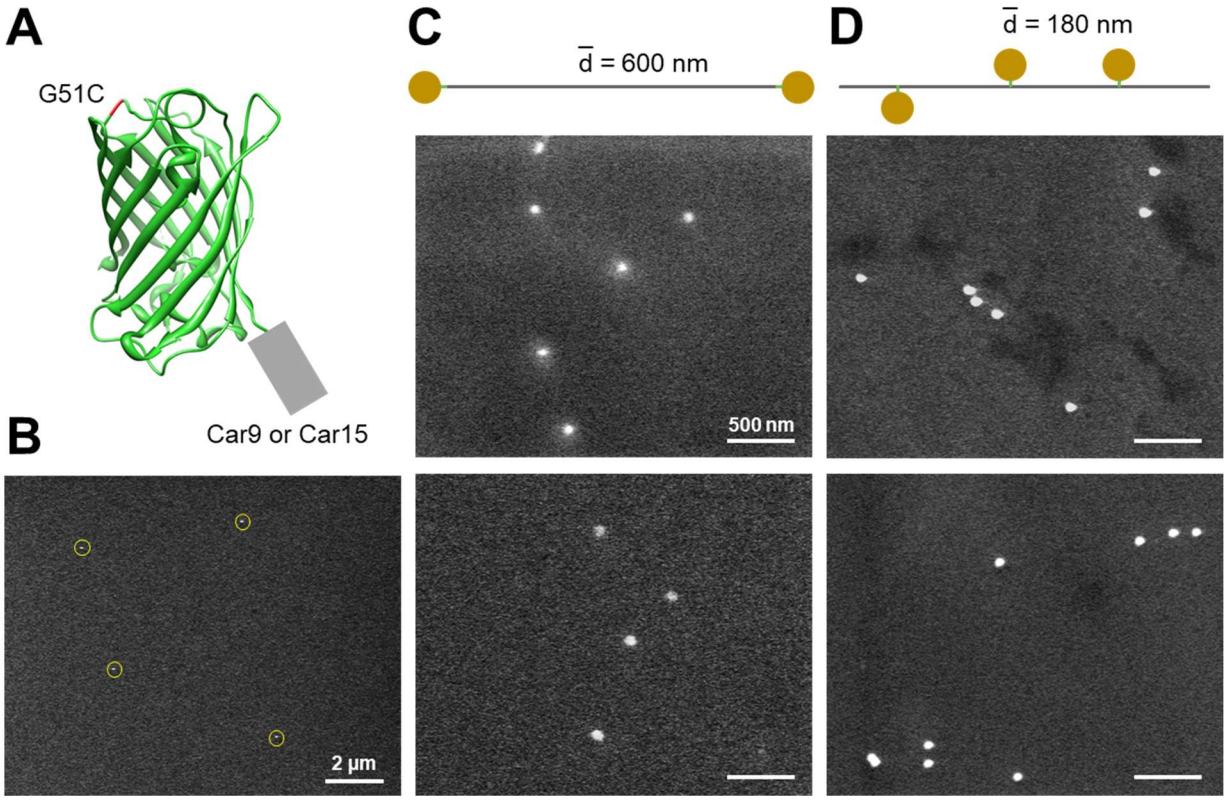

Figure 7: (A) Schematic of sfGFP(G51C)-Car9 and His-sfGFP(G51C)-Car15 showing relative location of G51C mutation and Car9 or Car15 SBP. (B) SEM images of Au (50 nm) with His-sfGFP(G51C)-Car15. (C) Schematic of SWNT end decorated with sfGFP(G51C)-Car9 scaffold and 50 nm Au and characteristic SEM images. (D) Schematic of SWNT wall decorated with His-sfGFP(G51C)-Car15 scaffold and 50 nm Au and characteristic SEM images.

Conclusions

In this study, we have shown that the Car9 and Car15 carbon binding peptides endow fluorescent proteins to which they are fused with the ability to selectively recognize SWNT ends and side

walls. By exploiting the host protein scaffold to display a carbon binding sequence together with a gold-binding peptide, or an engineered cysteine residue, at well-defined spatial locations, we further showed that it was possible to produce dual materials binders that support the selective conjugation of Au nanoparticles to the ends and sidewalls of SWNT. The approach is generic and should prove useful for the controlled and hierarchical assembly of other hybrid materials. It also holds promise for the creation of reconfigurable assemblies through the use of stimuli-responsive protein scaffolds.

Materials and Methods

DNA manipulations

Table 1: *E.* coli strains and plasmids used in this study

Strain or plasmid	Description	Source
E. coli strains		
Top 10	F- *endA*1 *recA*1 *hsdR*17 (r^-_k,m^+_k) λ^- *supE*44 *thi*1 *gyrA*96 *relA*1 ϕ80Δ*lac*Δ*M15* Δ(*lacZYA-argF*)U169 *deo*R	
SF100	F' Δ*lac*X74 *galE galK thi rpsL*(*strA*) Δ*phoA* Δ*ompT*	61
BL21(DE3)	B F^- *ompT gal dcm lon* $hsdS_B(r_B^-m_B^-)$ λ(DE3 [*lacI lacUV5-T7p07 ind1 sam7 nin5*]) $[malB^+]_{K\text{-}12}(\lambda^S)$	Novagen
Plasmids		
pBLN200	pBADXX derivative (ColE1) containing a multiple cloning site (MCS) suitable for placing genes under the control of the arabinose-inducible PBAD promoter. (Kan^r)	37
pBLN200-Car15	pBLN200 derivative encoding the Car15 SBP on a *Hin*dIII-*Xho*I fragment (Kan^r)	This study
pBLN200-sfGFP	pBLN200 derivative encoding sfGFP flanked on a *Nde*I-*Hin*dIII fragment (Kan^r)	This study
pBLN200-sfGFP-Car15	pBLN200 derivative encoding sfGFP-Car15 on a *Nde*I-*Xho*I fragment (Kan^r)	This study
pBLN200-Car9	pBLN200 derivative encoding the Car9 SBP on a *Hin*dIII-*Xho*I fragment (Kan^r)	40
pBLN200-His-mCherry-Car9	pBLN200 derivative encoding His-mCherry-Car9 on a *Nde*I-*Xho*I fragment (Kan^r)	40
pET-24a(+)	ColE1 cloning vector containing an MCS suitable for positioning genes under transcriptional control of the IPTG-inducible T7 promoter (Kan^r)	Novagen
pET-24a(+)-sfGFP	pET-24a(+) derivative encoding sfGFP on a *Nde*I-*Hin*dIII fragment (Kan^r)	This study
pET-24a(+)-sfGFP-Car9	pET-24a(+) derivative encoding sfGFP-Car9 on a *Nde*I-*Xho*I fragment (Kan^r)	38, 41
pET-24a(+)-sfGFP-Car15	pET-24a(+) derivative encoding sfGFP-Car15 on a *Nde*I-*Xho*I fragment (Kan^r)	This study

pET-24a(+)-His-mCherry-Car15	pET-24a(+) derivative encoding His-mCherry-Car15 on a *Nde*I-*Xho*I fragment (Kan^r)	This study
pET-22a(+)-Car9-sfGFP	pET-22a(+) derivative encoding Car9-sfGFP on a *Nde*I-*Xho*I fragment (Carb^r)	[41]
pET-22a(+)-His-sfGFP	pET-22a(+) derivative encoding His-sfGFP on a *Nde*I-*Xho*I fragment (Carb^r)	This study
pET-22a(+)-His-sfGFP-Car15	pET-22a(+) derivative encoding His-sfGFP-Car15 on a *Nde*I-*Xho*I fragment (Carb^r)	This study
pET-24a(+)-sfGFP::Car9-CT43	pET-24a(+) derivative encoding sfGFP::Car9-CT43 on a *Nde*I-*Xho*I fragment (Kan^r)	[46]
pET-24a(+)-sfGFP::Ag4-CT43	pET-24a(+) derivative encoding sfGFP::Ag4-CT43 on a *Nde*I-*Xho*I fragment (Kan^r)	This study
pET-24a(+)-sfGFP::Ag4-Car9	pET-24a(+) derivative encoding sfGFP::Ag4-Car9 on a *Nde*I-*Xho*I fragment (Kan^r)	This study
pET-24a(+)-sfGFP(G51C)::Car9-CT43	pET-24a(+) derivative encoding sfGFP::Car9-CT43 with Cys48-Ser/Gly51-Cys mutations in sfGFP on a *Nde*I-*Xho*I fragment (Kan^r)	This study
pET-24a(+)-sfGFP(G51C)-Car9	pET-24a(+) derivative encoding sfGFP-Car9 with Cys48-Ser/Gly51-Cys mutations in sfGFP on a *Nde*I-*Xho*I fragment (Kan^r)	This study
pET-24a(+)-sfGFP(G51C)-Car15	pET-24a(+) derivative encoding sfGFP-Car15 with Cys48-Ser/Gly51-Cys mutations in sfGFP on a *Nde*I-*Xho*I fragment (Kan^r)	This study
pET-22a(+)-His-sfGFP(G51C)-Car15	pET-22a(+) derivative encoding His-sfGFP-Car15 with Cys48-Ser/Gly51-Cys mutations in sfGFP on a *Nde*I-*Xho*I fragment (Carb^r)	This study

Plasmid pBLN200-Car15 (Table 1) was constructed by inserting a *Hin*dIII-*Xho*I cassette encoding a GGGS linker and the linear Car15 dodecamer[62] (RTYLPLPWMAAL) into the same sites of pBLN200.[63] The gene encoding sfGFP[64] was PCR-amplified on an *Nde*I-*Hin*dIII fragment and inserted into the same sites of pBLN200 and pBLN200-Car15 to yield plasmids pBLN200-sfGFP and pBLN200-sfGFP-Car15. Plasmid pBLN200-Car9 was constructed by inserting a *Hin*dIII-*Xho*I cassette encoding a GGGS linker and the linear Car9 dodecamer[62] (DSARGFKKPGKR) into the same sites of pBLN200.[63] The His-mCherry gene[43] was PCR-amplified on an *Nde*I-*Hin*dIII fragment and inserted into the same sites of pBLN200-Car9 to yield plasmid pBLN200-His-mCherry-Car9.

Plasmids pET-24a(+)-sfGFP, pET-24a(+)-sfGFP-Car9, and pET-24a(+)-sfGFP-Car15 were constructed by excising DNA segments encoding sfGFP, sfGFP-Car9, and sfGFP-Car15 from pBLN200-sfGFP, pBLN200-sfGFP-Car9, and pBLN200-sfGFP-Car15, on *Nde*I-*Hin*dIII (sfGFP), or *Nde*I-*Xho*I fragments (sfGFP-Car9 and sfGFP-Car15). DNA cassettes were inserted into the same sites of pET-24a(+) (Novagen) to yield plasmids pET-24a(+)-sfGFP, pET-24a(+)-sfGFP-Car9, and pET-24a(+)-sfGFP-Car15.

Plasmid pET24a(+)-His-mCherry-Car15 was constructed by inserting a *Nde*I-*Xho*I DNA fragment encoding His-mCherry from pBLN200-His-mCherry-Car9 into the same site of pET-24a(+)-sfGFP-Car15. Plasmid pET-22b(+)-His-sfGFP was constructed by introducing a *Nde*I-*Nco*I cassette encoding a hexahistidine tag followed by a GGGS linker and a TEV cleavage site into the same sites of pET-22b(+)-Car9-sfGFP.[41] Plasmid pET-22a(+)-His-sfGFP-Car15 was constructed by excising of a DNA fragment encompassing the 5' end of sfGFP and the Car15 dodecapeptide with *BsrG*I and *Xho*I and inserting it into the same sites of pET-22a(+)-His-sfGFP.

Plasmid pET-24a(+)-sfGFP::Ag4-Car9 was constructed as follows. Oligonucleotides (10 μM) encoding the Ag4 silver/gold binding peptide (NPSSLFRYLPSD)[50] (5'-GCTATAGTTGGATCCAACCCGAGCAGCCTGTTTTCGCTATCTGCCGAGCGATACTAG TTCATAGCG -3' and 5'-CGCATATGAACTAGTATCGCTCGGCAGATAGCGAAACAGGCTGCTCGGGTTGGATC CAACTATAGC-3') were annealed in boiling water for 10 minutes and allowed to cool to room temperature. The product was digested with *Bam*HI and *Spe*I and inserted in the same sites of pET-24a(+)-sfGFP::Car9-CT43[46] to yield pET-24a(+)-sfGFP::Ag4-CT43. Next, a fragment encompassing the sfGFP::Ag4 fusion was excised using *Nde*I and *Hin*dIII and ligated into the same sites of pET-24a(+)-sfGFP-Car9 to produce pET-24a(+)-sfGFP::Ag4-Car9.

The Cys48-Ser/Gly51-Cys mutations were introduced into pET24a(+)-sfGFP::Car9-CT43 by Quikchange mutagenesis using primer pair 5'-GCCAAGGTACCGGCAGTTTGCAAGTAGTGCTGATGAACTTCAGCGTCAGT-3' and 5'-ACTGACGCTGAAGTTCATCAGCACTACTTGCAAACTGCCGGTACCTTGGC-3'. A *Nde*I-*Kpn*I segment encoding the 5' end of sfGFP and encompassing the C48S/G51C mutations was excised from pET24a(+)-sfGFP(G51C)::Car9-CT43 using *Nde*I and *Kpn*I and inserted into the same sites of pET24a(+)-sfGFP-Car9, resulting in pET24a(+)-sfGFP(G51C)-Car9.

Plasmid pET-24a(+)-sfGFP(G51C)-Car15 was constructed through excision of a *Nde*I-*Hin*dIII DNA fragment encoding sfGFP(G51C) from pET-24a(+)-sfGFP(G51C)-Car9 and its insertion into the same sites of pET-24a(+)-sfGFP-Car15 resulting in pET-24a(+)-sfGFP(G51C)-Car15. A new restriction site, *BsmB*I, was introduced in plasmid pET-24a(+)-sfGFP(G51C)-Car15 at the 5' end of the gene encoding sfGFP(G51C)-Car15 using primer pair 5'-GACGTCTCCCATGCGTAAAGGCGAAGAG-3' and 5'-GACGTCTCCCATGGATGCGTAAAGGCGAAGAG-3' via Quikchange mutagenesis. The DNA fragment encoding sfGFP(G51C)-Car15 was excised from pET-24a(+)-sfGFP(G51C)-Car15 using *BsmB*I and *Xho*I, and inserted into the *Nco*I and *Xho*I sites of pET-22a(+)-His-sfGFP (*BsmB*I and *Nco*I have identical sticky ends, making the insertion possible) resulting in the plasmid pET-22a(+)-His-sfGFP(G51C)-Car15.

All constructs were verified by DNA sequencing and all DNA manipulations were conducted in Top10 cells (Table 1)

Protein expression and purification

Seed cultures (25 mL) of *E. coli* SF100 harboring plasmids pBLN200-sfGFP-Car15 or pBLN200-His-mCherry-Car9 (Table 1) were used to inoculate 500 mL of LB medium supplemented with 50 µg/mL kanamycin and cells were grown to mid-exponential phase (A_{600} of 0.4 to 0.6) at 37°C. Synthesis of sfGFP-Car15 and His-mCherry-Car9 was induced by addition of 2% L-Arabinose 10 min after cultures had been transferred to 25°C. After 6h of cultivation at the same temperature, cells were harvested by centrifugation at 7,000*g* for 5 min, resuspended in 35 mL of 20 mM Tris-HCl pH 7.5 (Buffer A) supplemented with 2 mM EDTA (Sigma), and disrupted by 6 rounds of sonication for 3 min at 30% duty cycle using a Branson sonifier. Lysates were clarified by centrifugation at 10,000*g* for 15 min. The sfGFP-Car15 lysate was immersed in a water bath at 80°C for 15 min and clarified by centrifugation at 14,000*g* for 15 min. Proteins sfGFP-Car15 and His-mCherry-Car9 were purified to near homogeneity by ion exchange chromatography on a Whatman DE52 anion exchange column equilibrated in Buffer A, as described.[65] Briefly, clarified lysate were loaded onto the column at ~1 mL/min, the resin was washed with 10 column volumes of Buffer A, and target proteins were eluted with a linear gradient of 0-250 mM NaCl in Buffer A over 60 min. The majority of the target proteins eluted at ~80 mM NaCl. After dialysis against 50 mM sodium phosphate buffer pH 7.5, proteins were aliquoted at a 10 µM final concentration and stored at -20°C.

BL21(DE3) (Table 1) cells harboring pET-24a(+) or pET-22a(+) derivatives were grown to mid-exponential phase as above, and recombinant protein expression was induced by addition of 500 µL of 1 M isopropyl β-D-thiogalactopyranoside (IPTG, Sigma). Cells were grown for an additional 4 h at 37 °C, harvested by centrifugation at 4000*g* for 10 min, and the pellet was resuspended in 35 mL of Buffer A supplemented with 2 mM EDTA and 1 mM phenylmethylsulfonyl fluoride (PMSF, Acros Organics). Cell were lysed and lysates clarified as above. Proteins sfGFP-Car9, sfGFP::Ag4-Car9, and sfGFP(G51C)-Car9 were purified to near homogeneity using silica affinity chromatography[41] essentially as described. Briefly, 6 g (~5 mL slurry) of Davisil 643 silica (Sigma) was washed 3 times with 15 mL of Buffer A to remove fines. Clarified lysates (35 mL) were added, and the mixture was loaded on a 1" diameter plastic column fitted with a two-way valve after 15 min of agitation on a roto-mixer operated at 60 rpm. Buffer A was gently added to the top of the column in 15 mL increments and pulled through the bed until the flow through was no longer green (~ 45 mL). Bound proteins were eluted with ~60 mL of 1 M Lysine in 20 mM Tris-HCl, pH 8.25. Purified proteins were dialyzed against Buffer A, aliquoted at 10 µM concentration, and stored at -20 °C.

His-mCherry-Car15, His-sfGFP, His-sfGFP-Car15, and His-sfGFP(G51C)-Car15 were purified by Ni-NTA affinity chromatography using a 5 mL column connected to a fast protein liquid chromatography (FPLC) system. To this end, cell paste from 500 mL culture prepared as above was lysed as described above in 35 mL of Buffer A supplemented with 10 mM imidazole (Alfa Aesar) and 1 mM PMSF. The lysate was clarified by centrifugation at 15,000*g* for 10 min and

loaded onto the Ni-NTA column, previously equilibrated with Buffer A, at a flow rate of 0.6 mL/min. The column was washed with 10 volumes of Buffer A supplemented with 20 mM imidazole and proteins were eluted with 250 mM imidazole in the same buffer. Successive elution fractions (5 mL) were assessed for purity using SDS-PAGE, pooled, dialyzed against Buffer A, and aliquoted at a 10 μM final concentration for storage at -20 °C.

Carbon nanotube resuspension

Sonication experiments – Approximately 1 mg of single-walled carbon nanotube (SWCNT) purchased from Sigma Aldrich (catalog #775533) were transferred to a 5 mL glass vial containing 2.7 mL of 50 mM phosphate buffer pH 7.5. The mixture was sonicated for 1.5 minutes on a Branson Sonifier 450 operated at 12W and 100% duty cycle using a micro-tipped wand. Next, 300 μL of 10 μM sfGFP-Car15 was added, and the solution was sonicated as above for another 1.5 minutes. Vials were immersed in a mixture of EtOH and ice to minimize heat-induced protein denaturation. Experiments labeling SWCNT with sfGFP-Car15 and His-mCherry-Car9 simultaneously were performed as above except that the final concentration of each protein was 1 μM and 0.5 μM, respectively, and the length of the sonication step was increased to 3 minutes. Samples were centrifuged at 14,000*g* for 15 minutes to remove larger aggregates or used as prepared.

Dialysis experiments – Solutions of metallic and semiconducting SWCNT (90% purity, 0.01 mg/mL concentration) were purchased from NanoIntegris (Boisbriand, Quebec, Canada). The proprietary detergent stabilizing the nanotubes was replaced by sodium cholate by mixing SWCNT (750 μL) with the same volume of 2 wt% Na-Cholate (Sigma) in Buffer A, and agitating the solution on a Dynabeads rotary mixer (Invitrogen) for 20 min at 60 rpm and 21ºC. Proteins (400 μL of 10 μM stock solutions) were added and mixing continued for 20 min. The solution was transferred to Snakeskin® Dialysis Tubing, 10,000 MWCO (Thermo Scientific) and dialyzed 12 hours at 10 °C against 0.5 L Buffer A to remove the surfactant. The buffer was exchanged twice, resulting in a total dialysis time of 36 hours. The final concentration of SWCNT and protein was 0.004 mg/mL and 2 μM but varied slightly due to the dialysis step.

Fluorescence microscopy

Protein-treated SWCNT samples were imaged by fluorescence microscopy on a Nikon Eclipse TE2000-U microscope at 90x magnification using a 60x oil-immersion objective. Samples prepared with sfGFP (λ_{ex}=485 nm, λ_{em}=510 nm) variants were illuminated with a 480/40 nm wavelength filter and fluorescence was collected in the 510-560 nm window. Samples prepared with mCherry (λ_{ex}=587 nm, λ_{em}=610 nm) variants were illuminated with a 520/40 nm wavelength filter and fluorescence was collected in the 600-660 nm window. Samples prepared by sonication were diluted 4-fold with 50 mM phosphate buffer pH 7.5. Aliquots (10 μL) were deposited on a glass microscope slide and covered with a glass coverslip. Samples prepared by dialysis were first incubated with either silica (for Car9-tagged variants) or Ni-NTA (for His-tagged variants) to remove excess, unbound protein from solution. Briefly, 100 μL of sample was added to 10 μL either silica (Davisil 643, Sigma) or Ni-NTA (HisPur® Ni-NTA, Thermo Scientific) resin, both washed with Buffer A, and incubated for 10 min without agitation. 10 μL of the supernatant was

deposited on a glass microscope slide and covered with a glass coverslip. Glass slides and coverslips were rinsed with EtOH and ddH_2O before samples were added.

Gold nanoparticles-solid binding proteins interactions

Citrate-capped gold nanoparticles 5 nm in diameter (catalog #G1402) in 1.6 mM trisodium citrate, 0.26 mM potassium carbonate, and 3 mM sodium azide and at a concentration of $5.5x10^{13}$ particles/mL (given by manufacturer), calculated to be $9.1x10^{-5}$ μM using Avogadro's number, were purchased from Sigma-Aldrich (St. Louis, MO). Citrate-capped 50 nm diameter gold nanoparticles (50 nm Citrate NanoXact Gold, catalog #DAC1278) in 2 mM sodium citrate and at a concentration of 0.05 mg/mL (given by manufacturer), calculated to be $6.6x10^{-5}$ μM using density of 50 nm gold nanoparticles as 19.32 g/cm^3, were purchased from nanoComposix (San Diego, CA). UV-Visible spectra of protein-gold nanoparticle mixtures were collected on a Beckman Coulter DU 640 spectrophotometer using 1 mL samples consisting of 900 μL of the indicated protein at 0.5 μM concentration and 100 μL of nanoparticles after gentle mixing for 30 min at room temperature. The fluorescence spectra of the same samples were recorded on a Hitachi F-4500 fluorescence spectrophotometer with an excitation wavelength of 485 nm (sfGFP) and excitation and emission slits set at 2.5 nm. Metal quenching of sfGFP fluorescence by gold nanoparticles was calculated for each protein by measuring the fluorescence emission at 510 nm of solutions containing or lacking gold nanoparticles, and taking the ratio of these values.

To quantify how much protein was bound to gold, mixtures were centrifuged for 15 min at 16,800*g* and supernatants were transferred to a black 96-wells microplate (Greiner) along with nanoparticle-free controls. The fluorescence was measured at 510 nm on a SpectraMax M5 microplate reader (Molecular Devices) with excitation at 475 nm and a cutoff wavelength of 495 nm. The reduction in fluorescence between supernatants and controls was used to calculate the fraction of protein bound to gold nanoparticles.

To test the dual binding capabilities of Car9-tagged proteins, 200 μL of Davisil grade 646 silica (Sigma) was added to a microcentrifuge tube, washed with Buffer A, and all supernatant buffer was removed. 1 mL of 0.5 μM sfGFP, sfGFP-Car9, sfGFP::Ag4-Car9, or sfGFP(G51C)-Car9 were added to the tube and gently mixed for 3 min. 100 μL of either 5 nm or 50 nm citrate capped gold nanoparticles (described above) were added and the mixture was gently mixed for 30 min. After allowing the silica bed to settle for 2-3 min, the supernatants were collected and the absorbance spectra were collected on a Beckman Coulter DU 640 spectrophotometer using 1 mL samples.

To test the dual binding capabilities of Car15-tagged proteins, 100 μL of Ni-NTA (HisPur® Ni-NTA, Thermo Scientific) resin was added to a microcentrifuge tube, washed with buffer A, and all supernatant was removed. 1 mL of His-sfGFP-Car15 or His-sfGFP(G51C)-Car15 was added to the tube gently mixed for 3 min. 100 μL of either 5 nm or 50 nm citrate capped gold nanoparticles (described above) were added and the mixture was gently mixed for 30 min. After allowing the Ni-NTA resin to settle for 2-3 min, the supernatants were collected and the absorbance spectra were collected on a Beckman Coulter DU 640 spectrophotometer using 1 mL samples.

Scanning Electron Microscopy

Protein-stabilized SWCNT (80 µL) prepared by dialysis were mixed with 20 µL of the indicated gold nanoparticle solution for 30 min at room temperature on a rotary mixer operated at 60 rpm. Aliquots (30 µL) were deposited on a silicon wafer and allowed to stand at room temperature for 5 min. Excess moisture was wicked away with filter paper and the wafer was washed 4 times with ddH_2O water by dunking, and wicking away excess liquid between each washing step. Wafers were allowed to dry overnight on filter paper in a petri dish placed in a fume hood and samples were imaged on a FEI Sirion XL30 scanning electron microscope at an accelerating voltage of 5 kV.

References

1. Iijima, S. Helical microtubules of graphitic carbon. *Nature* **354**, 56 (1991).
2. Geim, A.K. & Novoselov, K.S. The rise of graphene. *Nature Materials* **6**, 183 (2007).
3. Odom, T.W., Huang, J.-L., Kim, P. & Lieber, C.M. Atomic structure and electronic properties of single-walled carbon nanotubes. *Nature* **391**, 62-64 (1998).
4. Tombler, T.W. et al. Reversible electromechanical characteristics of carbon nanotubes under local-probe manipulation. *Nature* **405**, 769-772 (2000).
5. Bellucci, S. Carbon nanotubes: physics and applications. *physica status solidi (c)* **2**, 34-47 (2005).
6. Hong, S. & Myung, S. A flexible approach to mobility. *Nature Nanotechnology* **2**, 207 (2007).
7. Brady, G.J. et al. Quasi-ballistic carbon nanotube array transistors with current density exceeding Si and GaAs. *Science Advances* **2** (2016).
8. Fawad, I., Michael, J.R. & Ton, P. Shortened carbon nanotubes and their influence on the electrical properties of polymer nanocomposites. *Journal of Composite Materials* **46**, 1313-1322 (2011).
9. Yang, Z. et al. Carbon Nanotubes Bridged with Graphene Nanoribbons and Their Use in High-Efficiency Dye-Sensitized Solar Cells. *Angewandte Chemie International Edition* **52**, 3996-3999 (2013).
10. Rosi, N.L. & Mirkin, C.A. Nanostructures in Biodiagnostics. *Chemical Reviews* **105**, 1547-1562 (2005).
11. Yum, K. et al. Boronic Acid Library for Selective, Reversible Near-Infrared Fluorescence Quenching of Surfactant Suspended Single-Walled Carbon Nanotubes in Response to Glucose. *ACS Nano* **6**, 819-830 (2012).
12. Baptista, F.R., Belhout, S.A., Giordani, S. & Quinn, S.J. Recent developments in carbon nanomaterial sensors. *Chemical Society Reviews* **44**, 4433-4453 (2015).
13. Calvaresi, M. & Zerbetto, F. The Devil and Holy Water: Protein and Carbon Nanotube Hybrids. *Accounts of Chemical Research* **46**, 2454-2463 (2013).
14. Bradley, K., Briman, M., Star, A. & Grüner, G. Charge Transfer from Adsorbed Proteins. *Nano Letters* **4**, 253-256 (2004).
15. Allen, B.L., Kichambare, P.D. & Star, A. Carbon Nanotube Field-Effect-Transistor-Based Biosensors. *Advanced Materials* **19**, 1439-1451 (2007).
16. Premkumar, T., Mezzenga, R. & Geckeler, K.E. Carbon Nanotubes in the Liquid Phase: Addressing the Issue of Dispersion. *Small* **8**, 1299-1313 (2012).
17. Karousis, N., Tagmatarchis, N. & Tasis, D. Current Progress on the Chemical Modification of Carbon Nanotubes. *Chemical Reviews* **110**, 5366-5397 (2010).
18. Hirsch, A. Functionalization of Single-Walled Carbon Nanotubes. *Angewandte Chemie International Edition* **41**, 1853-1859 (2002).
19. Karajanagi, S.S., Vertegel, A.A., Kane, R.S. & Dordick, J.S. Structure and Function of Enzymes Adsorbed onto Single-Walled Carbon Nanotubes. *Langmuir* **20**, 11594-11599 (2004).
20. Kurppa, K. et al. Controlled Hybrid Nanostructures through Protein-Mediated Noncovalent Functionalization of Carbon Nanotubes. *Angewandte Chemie International Edition* **46**, 6446-6449 (2007).
21. Liu, P. Modifications of carbon nanotubes with polymers. *European Polymer Journal* **41**, 2693-2703 (2005).
22. Welsher, K. et al. A route to brightly fluorescent carbon nanotubes for near-infrared imaging in mice. *Nat Nano* **4**, 773-780 (2009).
23. Hertel, T. et al. Spectroscopy of Single- and Double-Wall Carbon Nanotubes in Different Environments. *Nano Letters* **5**, 511-514 (2005).

24. Zhao, Y.-L. & Stoddart, J.F. Noncovalent Functionalization of Single-Walled Carbon Nanotubes. *Accounts of Chemical Research* **42**, 1161-1171 (2009).
25. Bergler, F.F., Stahl, S., Goy, A., Schöppler, F. & Hertel, T. Substrate-Mediated Cooperative Adsorption of Sodium Cholate on (6,5) Single-Wall Carbon Nanotubes. *Langmuir* **32**, 9598-9603 (2016).
26. Oliveira, S.F. et al. Protein functionalized carbon nanomaterials for biomedical applications. *Carbon* **95**, 767-779 (2015).
27. Dai, H. Carbon Nanotubes: Synthesis, Integration, and Properties. *Accounts of Chemical Research* **35**, 1035-1044 (2002).
28. Yoshimura, S.H., Khan, S., Maruyama, H., Nakayama, Y. & Takeyasu, K. Fluorescence Labeling of Carbon Nanotubes and Visualization of a Nanotube−Protein Hybrid under Fluorescence Microscope. *Biomacromolecules* **12**, 1200-1204 (2011).
29. Sarikaya, M., Tamerler, C., Jen, A.K.Y., Schulten, K. & Baneyx, F. Molecular Biomimetics: Nanotechnology Through Biology. *Nat. Mater.* **2**, 577 (2003).
30. Su, Z., Leung, T. & Honek, J.F. Conformational Selectivity of Peptides for Single-Walled Carbon Nanotubes. *The Journal of Physical Chemistry B* **110**, 23623-23627 (2006).
31. Lee, Y.J. et al. Fabricating Genetically Engineered High-Power Lithium-Ion Batteries Using Multiple Virus Genes. *Science* **324**, 1051 (2009).
32. Zheng, L., Jain, D. & Burke, P. Nanotube−Peptide Interactions on a Silicon Chip. *The Journal of Physical Chemistry C* **113**, 3978-3985 (2009).
33. Pender, M.J., Sowards, L.A., Hartgerink, J.D., Stone, M.O. & Naik, R.R. Peptide-Mediated Formation of Single-Wall Carbon Nanotube Composites. *Nano Letters* **6**, 40-44 (2006).
34. Wang, S. et al. Peptides with selective affinity for carbon nanotubes. *Nat Mater* **2**, 196-200 (2003).
35. Inoue, I. et al. A novel bifunctional protein supramolecule for construction of carbon nanotube-titanium hybrid material. *Chemical Communications* **47**, 12649-12651 (2011).
36. Coyle, B.L., Zhou, W. & Baneyx, F. Protein-aided mineralization of inorganic nanostructures. (Caister Academic Press: Norwich, UK, 2013).
37. Coyle, B.L., Rolandi, M. & Baneyx, F. Carbon-Binding Designer Proteins that Discriminate between sp2- and sp3-Hybridized Carbon Surfaces. *Langmuir* **29**, 4839-4846 (2013).
38. Coyle, B.L. & Baneyx, F. Direct and reversible immobilization and microcontact printing of functional proteins on glass using a genetically appended silica-binding tag. *Chemical Communications* **52**, 7001-7004 (2016).
39. Yang, W., Hellner, B. & Baneyx, F. Self-Immobilization of Car9 Fusion Proteins within High Surface Area Silica Sol–Gels and Dynamic Control of Protein Release. *Bioconjugate Chemistry* **27**, 2450-2459 (2016).
40. Coyle, B.L. & Baneyx, F. A cleavable silica-binding affinity tag for rapid and inexpensive protein purification. *Biotechnology and Bioengineering* **111**, 2019-2026 (2014).
41. Soto-Rodríguez, J., Coyle, B.L., Samuelson, A., Aravagiri, K. & Baneyx, F. Affinity purification of Car9-tagged proteins on silica matrices: Optimization of a rapid and inexpensive protein purification technology. *Protein Expression and Purification* **135**, 70-77 (2017).
42. Pedelacq, J.-D., Cabantous, S., Tran, T., Terwilliger, T.C. & Waldo, G.S. Engineering and characterization of a superfolder green fluorescent protein. *Nat Biotech* **24**, 79-88 (2006).
43. Shaner, N.C. et al. Improved monomeric red, orange and yellow fluorescent proteins derived from Discosoma sp. red fluorescent protein. *Nat Biotech* **22**, 1567-1572 (2004).
44. Lu, K.L. et al. Mechanical damage of carbon nanotubes by ultrasound. *Carbon* **34**, 814-816 (1996).

45. Crowe, J. et al. in Protocols for Gene Analysis. (ed. A.J. Harwood) 371-387 (Humana Press, Totowa, NJ; 1994).
46. Swift, B.J.F., Shadish, J.A., DeForest, C.A. & Baneyx, F. Streamlined Synthesis and Assembly of a Hybrid Sensing Architecture with Solid Binding Proteins and Click Chemistry. *Journal of the American Chemical Society* **139**, 3958-3961 (2017).
47. Aili, D. & Stevens, M.M. Bioresponsive peptide-inorganic hybrid nanomaterials. *Chemical Society Reviews* **39**, 3358-3370 (2010).
48. Uvdal, K., Bodö, P. & Liedberg, B. l-cysteine adsorbed on gold and copper: An X-ray photoelectron spectroscopy study. *Journal of Colloid and Interface Science* **149**, 162-173 (1992).
49. Lynch, I. & Dawson, K.A. Protein-nanoparticle interactions. *Nano Today* **3**, 40-47 (2008).
50. Naik, R.R., Stringer, S.J., Agarwal, G., Jones, S.E. & Stone, M.O. Biomimetic Synthesis and Patterning of Silver Nanoparticles. *Nat. Mater.* **1**, 169 (2002).
51. Hutter, E. & Fendler, J.H. Exploitation of Localized Surface Plasmon Resonance. *Advanced Materials* **16**, 1685-1706 (2004).
52. Liu, X., Atwater, M., Wang, J. & Huo, Q. Extinction coefficient of gold nanoparticles with different sizes and different capping ligands. *Colloids and Surfaces B: Biointerfaces* **58**, 3-7 (2007).
53. Larson-Smith, K. & Pozzo, D.C. Pickering Emulsions Stabilized by Nanoparticle Surfactants. *Langmuir* **28**, 11725-11732 (2012).
54. Brewer, S.H., Glomm, W.R., Johnson, M.C., Knag, M.K. & Franzen, S. Probing BSA Binding to Citrate-Coated Gold Nanoparticles and Surfaces. *Langmuir* **21**, 9303-9307 (2005).
55. Nath, N. & Chilkoti, A. A Colorimetric Gold Nanoparticle Sensor To Interrogate Biomolecular Interactions in Real Time on a Surface. *Analytical Chemistry* **74**, 504-509 (2002).
56. Walkey, C.D., Olsen, J.B., Guo, H., Emili, A. & Chan, W.C.W. Nanoparticle Size and Surface Chemistry Determine Serum Protein Adsorption and Macrophage Uptake. *Journal of the American Chemical Society* **134**, 2139-2147 (2012).
57. Kaufman, E.D. et al. Probing Protein Adsorption onto Mercaptoundecanoic Acid Stabilized Gold Nanoparticles and Surfaces by Quartz Crystal Microbalance and ζ-Potential Measurements. *Langmuir* **23**, 6053-6062 (2007).
58. Ghosh, S.K. & Pal, T. Interparticle Coupling Effect on the Surface Plasmon Resonance of Gold Nanoparticles: From Theory to Applications. *Chemical Reviews* **107**, 4797-4862 (2007).
59. Li, Z., Jin, R., Mirkin, C.A. & Letsinger, R.L. Multiple thiol-anchor capped DNA–gold nanoparticle conjugates. *Nucleic Acids Research* **30**, 1558-1562 (2002).
60. Tan, Y.N., Lee, J.Y. & Wang, D.I.C. Uncovering the Design Rules for Peptide Synthesis of Metal Nanoparticles. *J. Am. Chem. Soc.* **132**, 5677 (2010).
61. Baneyx, F. & Georgiou, G. In vivo degradation of secreted fusion proteins by the Escherichia coli outer membrane protease OmpT. *Journal of Bacteriology* **172**, 491-494 (1990).
62. Coyle, B.L., Rolandi, M. & Baneyx, F. Carbon-binding designer proteins that discriminate between sp2- and sp3-hybridized carbon surfaces. *Langmuir* **29**, 4839-4846 (2013).
63. Nannenga, B.L. & Baneyx, F. Reprogramming chaperone pathways to improve membrane protein expression in Escherichia coli. *Protein Sci.* **20**, 1411-1420 (2011).
64. Pedelacq, J.D., Cabantous, S., Tran, T., Terwilliger, T.C. & Waldo, G.S. Engineering and characterization of a superfolder green fluorescent protein. *Nat. Biotechnol.* **24**, 79-88 (2006).
65. Coyle, B.L. & Baneyx, F. Direct and reversible immobilization and microcontact printing of functional proteins on glass using a genetically appended silica-binding tag. *Chem. Commun.* **52**, 7001-7004 (2016).

Supplementary Figures

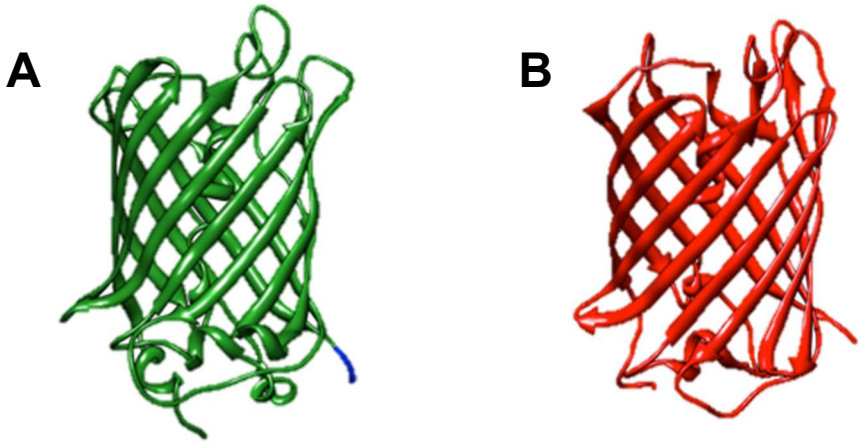

Figure S1: Ribbon structure of (A) sfGFP and (B) mCherry

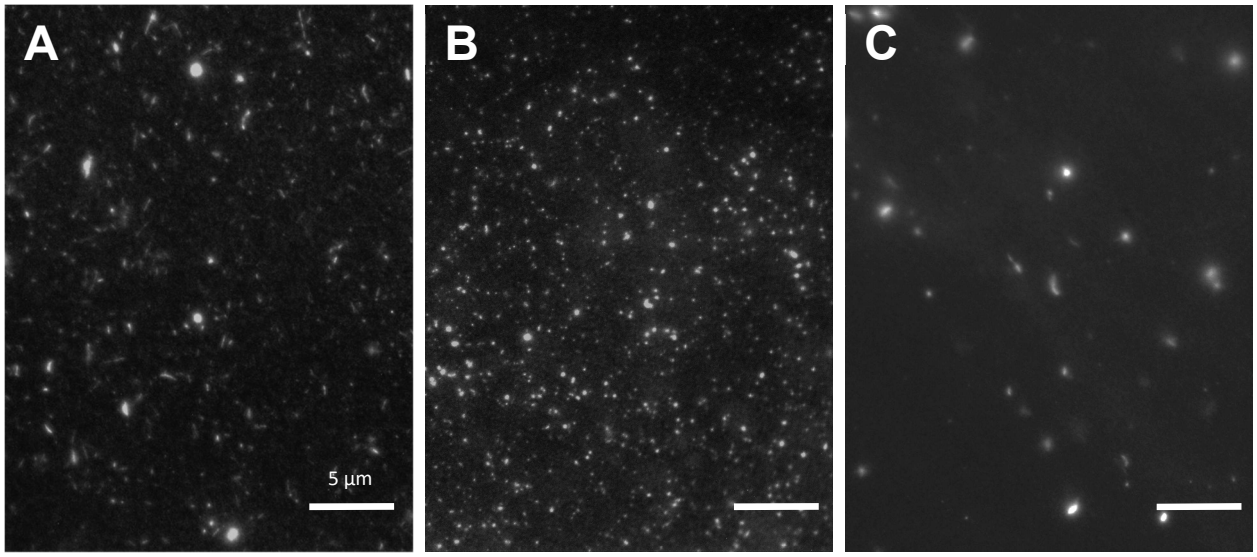

Figure S2: Fluorescent microscopy images (90x mag) of SWNT from dry powder resuspended by sfGFP-Car15 (λ_{ex}=473 nm) showing nanotube damage by sonication (A) 3 min sonication with tip #1 (B) 3 min sonication with tip #2 (C) 10 min bath sonication

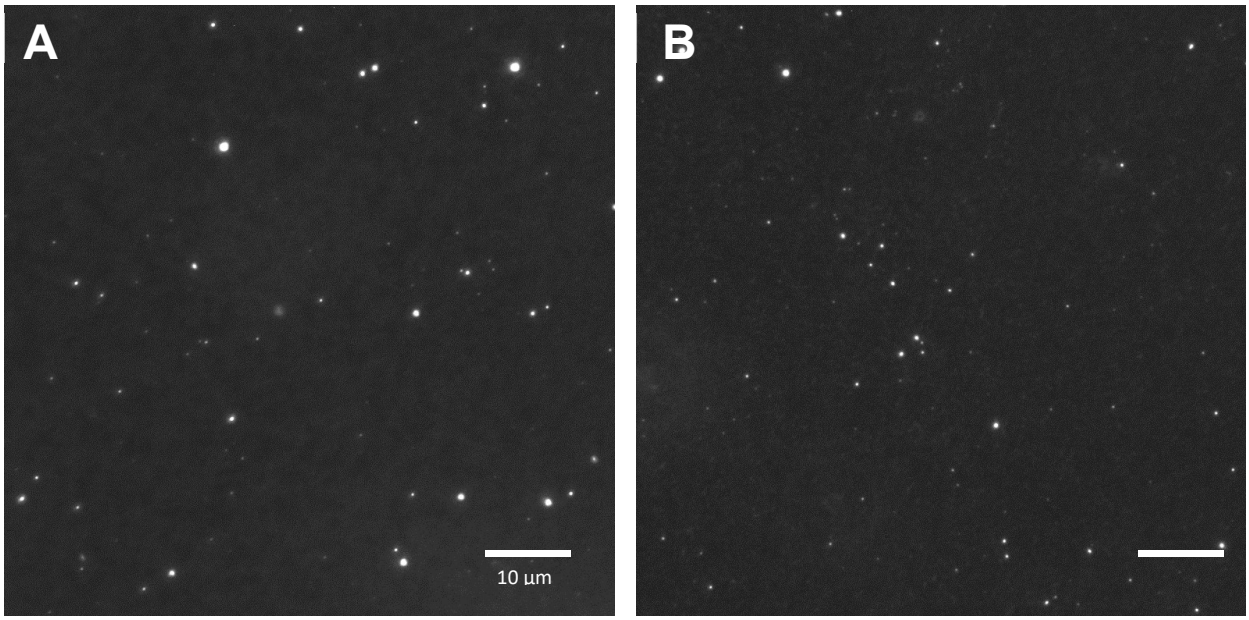

Figure S3: Fluorescent microscopy images (90x mag) of SWNT resuspended by sfGFP-Car9 through ligand exchange (λ_{ex}=473 nm) showing similar punctuated fluorescence for (A) semiconducting SWNT or (B) metallic SWNT

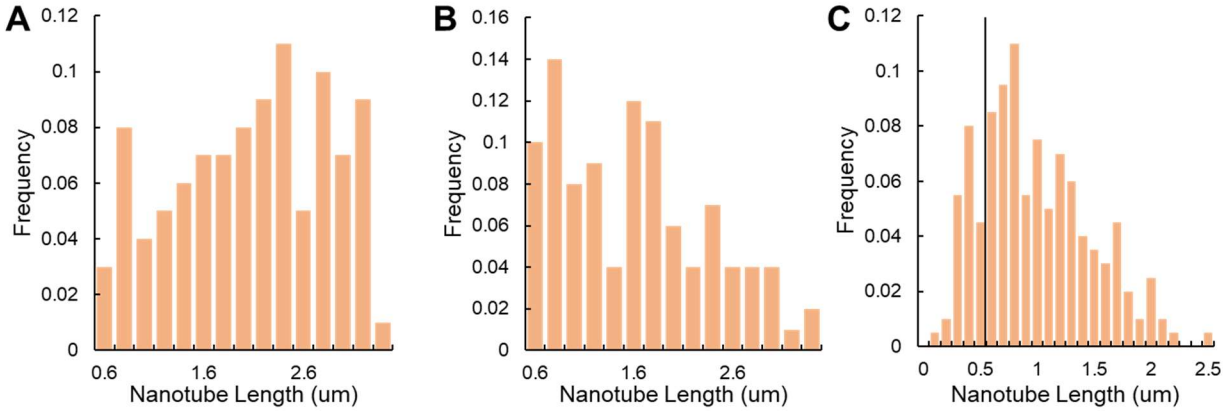

Figure S4: Length histograms of CNT's (A) From fluorescent microscopy images of semiconducting SWNT functionalized via ligand exchange by sfGFP-Car9 (B) From fluorescent microscopy images of metallic SWNT functionalized via ligand exchange by sfGFP-Car9 (C) Length histogram of pure SWNT from NanoIntegris with line noting diffraction limit of fluorescent microscopy (average length 1 ± 0.5 µm)

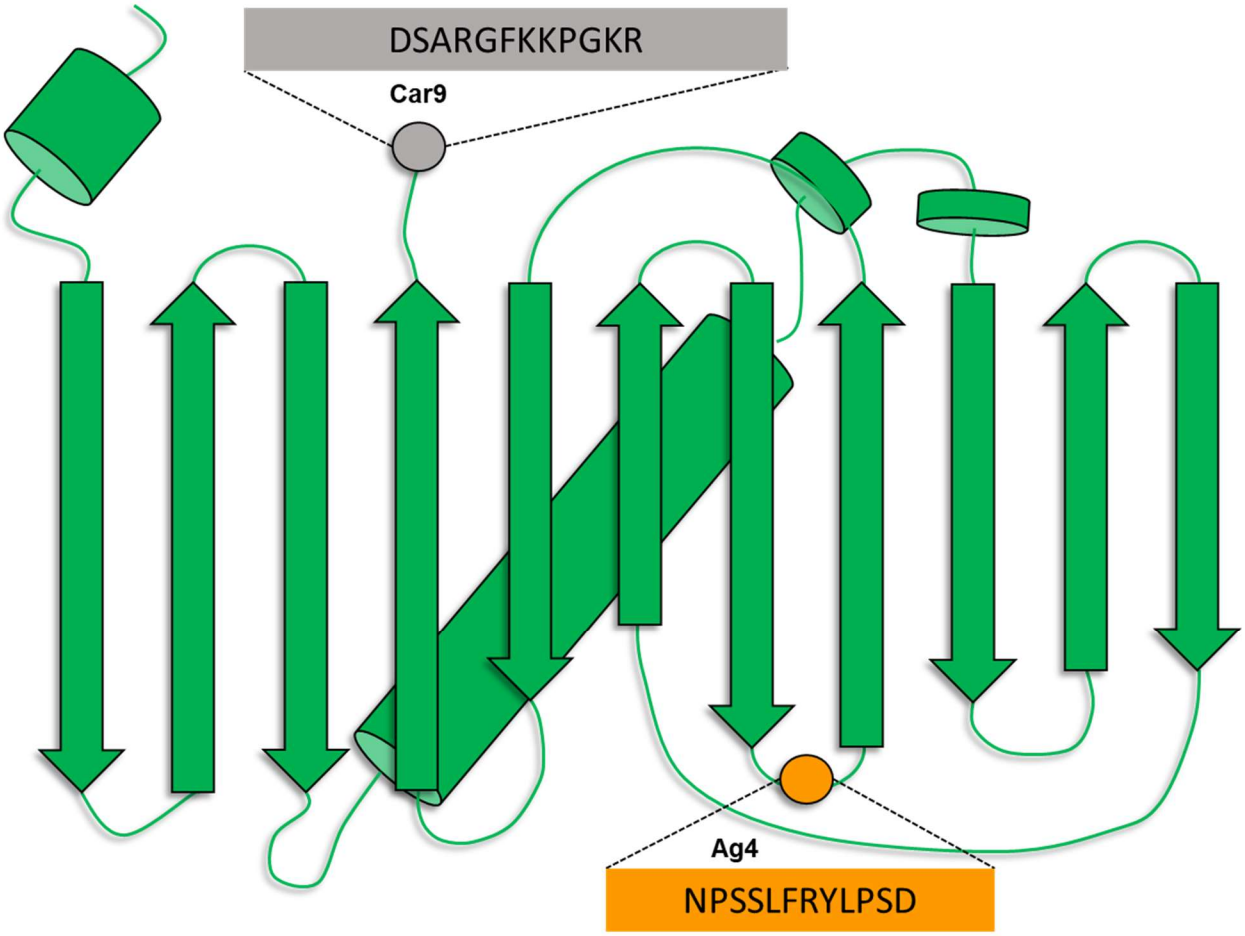

Figure S5: Cartoon structure of sfGFP showing the arrangement of β-strands and α-helices and the insertion locations and amino acid compositions of the Car9 and Ag4 solid-binding sequences.

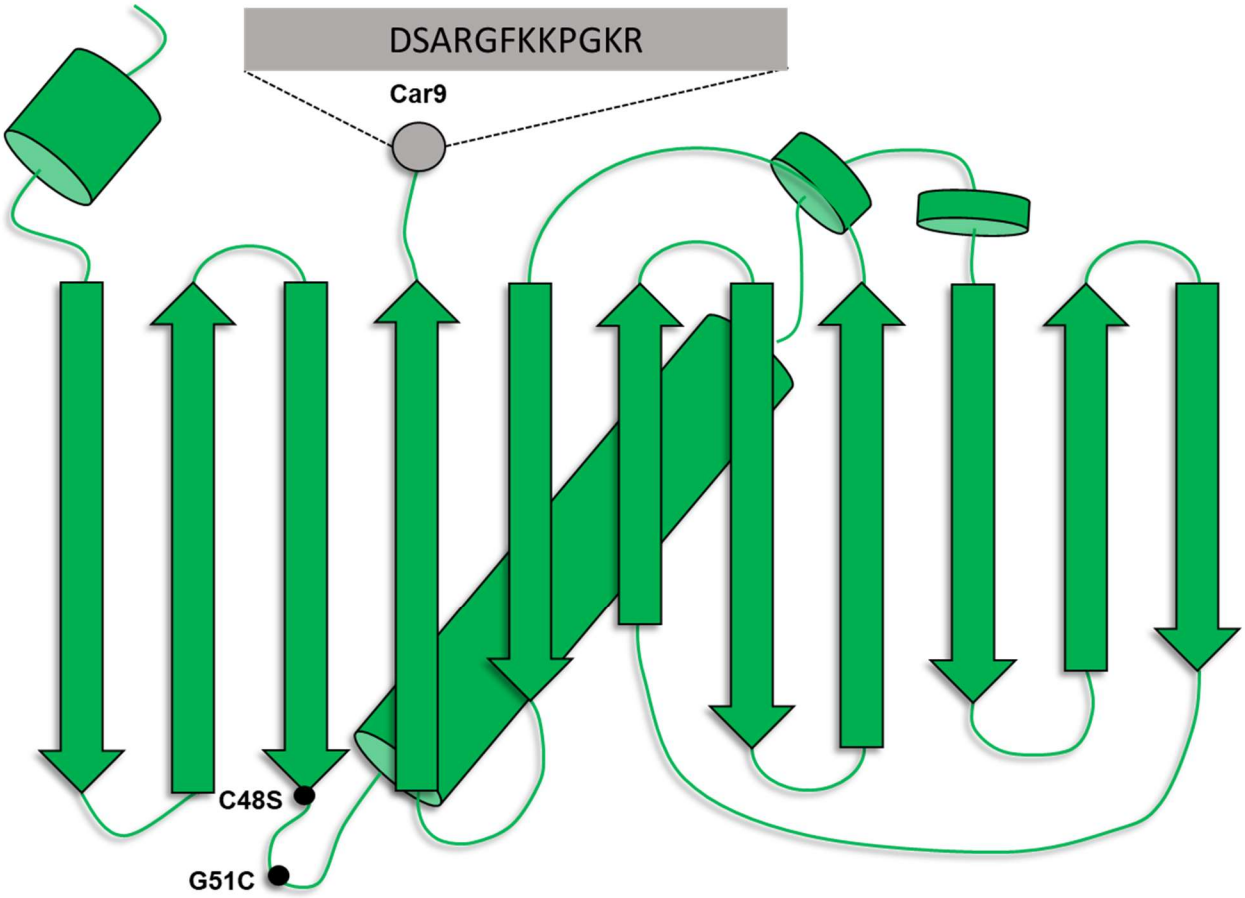

Figure S6: Cartoon structure of sfGFP showing the arrangement of β-strands and α-helices and the insertion locations and amino acid compositions of the Car9 solid-binding sequence and the Cys48-Ser/Gly51-Cys mutations.

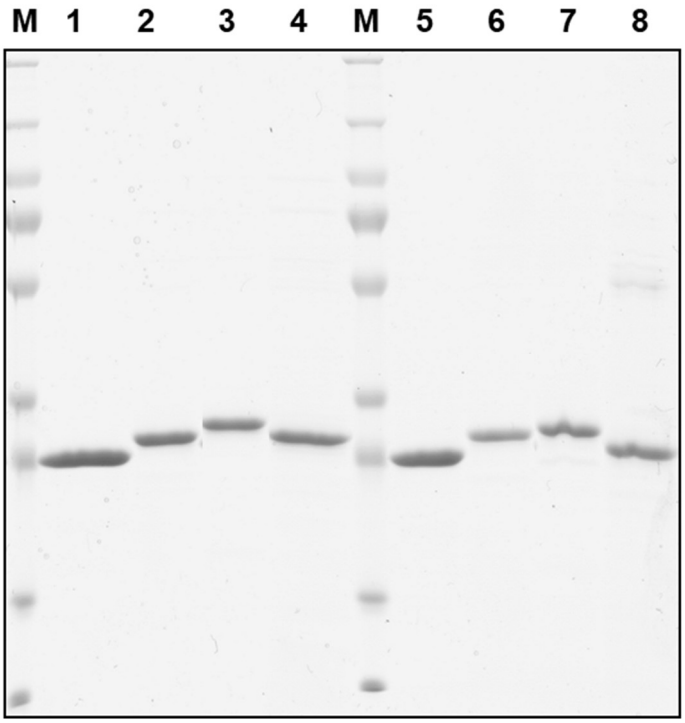

Figure S7: SDS-PAGE analysis of purified proteins under reducing (lane 1-4) or non-reducing conditions (lane 5-8) sfGFP (lane 1, 5), sfGFP-Car9 (lane 2, 6), sfGFP::Ag4-Car9 (lane 3, 7), sfGFP(G51C)-Car9 (lane 4, 8). Proteins with the Car9 SBP were purified by silica affinity chromatography. sfGFP was purified via ion exchange chromatography. 6x-His tagged proteins were purified by Ni-NTA affinity chromatography. Lane M contains molecular mass markers.

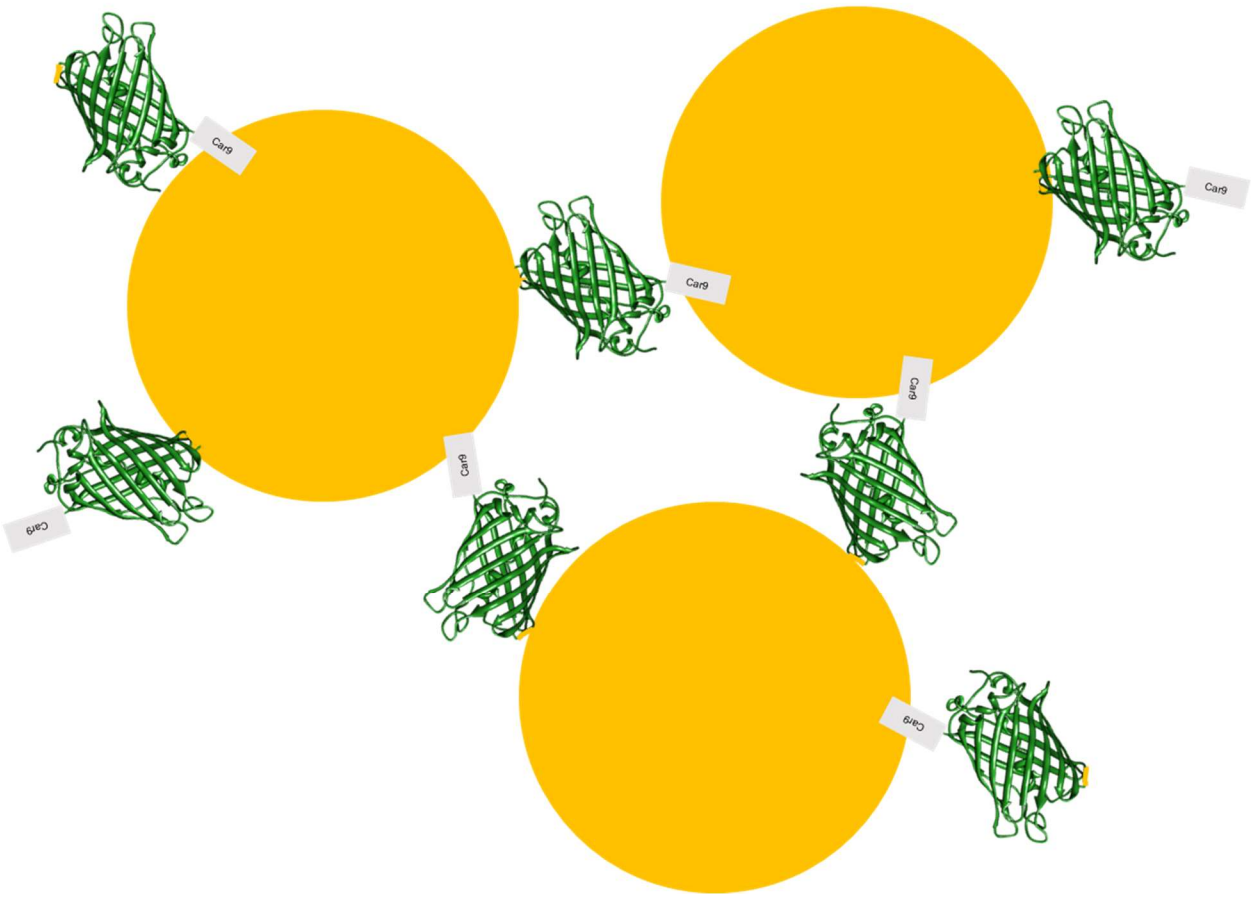

Figure S8: Cartoon schematic of sfGFP(G51C)-Car9 inducing 50 nm Au nanoparticle aggregation by binding both through Cys51 and Car9 (not to scale)

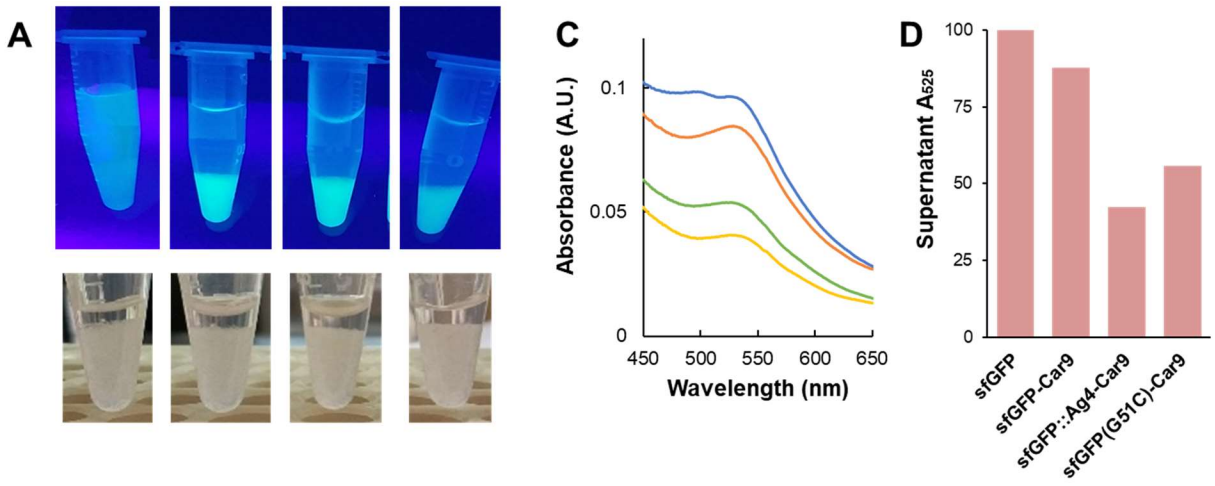

Figure S9: (A) sfGFP variants mixed with silica beads and photographed under 365 nm light [left to right sfGFP, sfGFP-Car9, sfGFP::Ag4-Car9, sfGFP(G51C)-Car9]. (B) Silica beads after protein and Au (5 nm) incubation. (C) Absorbance spectra of supernatants from B [sfGFP (blue), sfGFP-Car9 (red), sfGFP::Ag4-Car9 (yellow), sfGFP(G51C)-Car9 (green)]. (D) Percent Au (5 nm) remaining in supernatant after incubation with protein and silica as measured by absorbance at 525 nm.

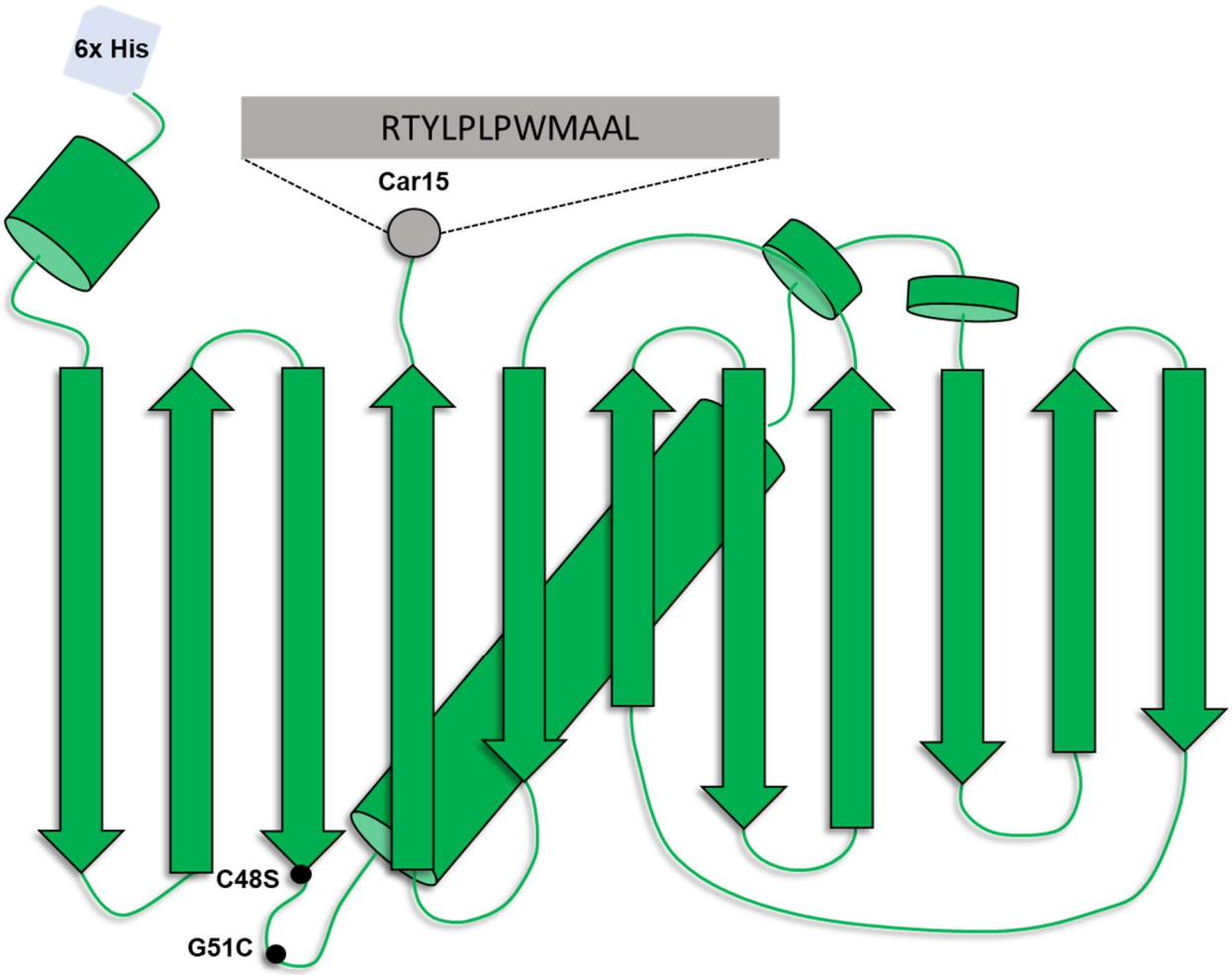

Figure S10: Cartoon structure of sfGFP showing the arrangement of β-strands and α-helices and the insertion locations and amino acid compositions of the 6x-histidine tag, Car15 solid-binding sequence, and the Cys48-Ser/Gly51-Cys mutations.

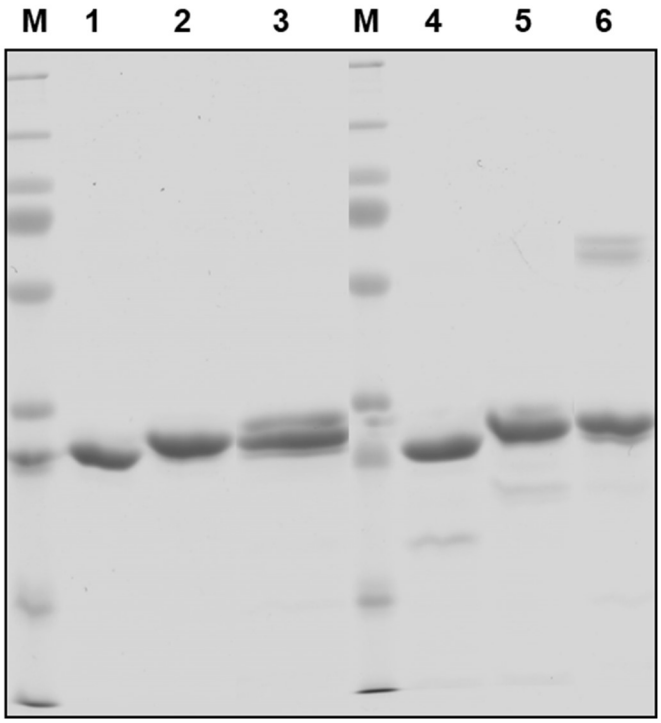

Figure S11: SDS-PAGE analysis of purified proteins under reducing (lane 1-3) or non-reducing conditions (lane 4-6) sfGFP (lane 1, 4), His-sfGFP (lane 2, 5), His-sfGFP(G51C)-Car15 (lane 3, 6). sfGFP was purified via ion exchange chromatography. 6x-His tagged proteins were purified by Ni-NTA affinity chromatography. Lane M contains molecular mass markers.

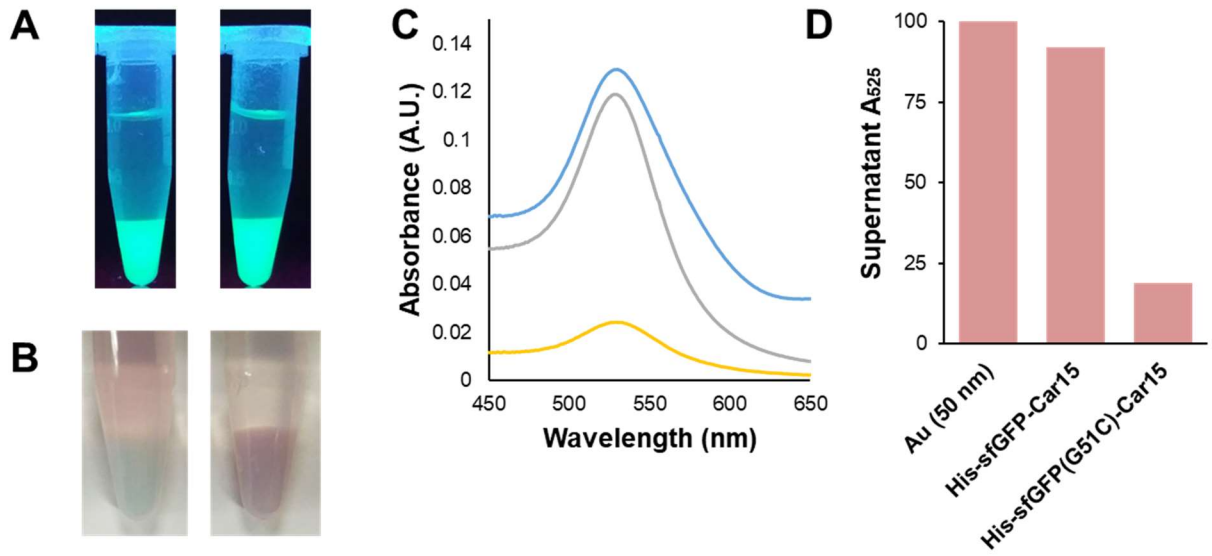

Figure S12: (A) sfGFP variants mixed with Ni-NTA beads and photographed under 365 nm light [His-sfGFP-Car15, His-sfGFP(G51C)-Car15]. (B) Ni-NTA beads after protein and Au (50 nm) incubation. (C) Absorbance spectra of supernatants from B [Au 50 nm (blue), His-sfGFP-Car15 (gray), His-sfGFP(G51C)-Car15 (yellow)]. (D) Percent Au (50 nm) remaining in supernatant after incubation with protein and Ni-NTA as measured by absorbance at 525 nm.

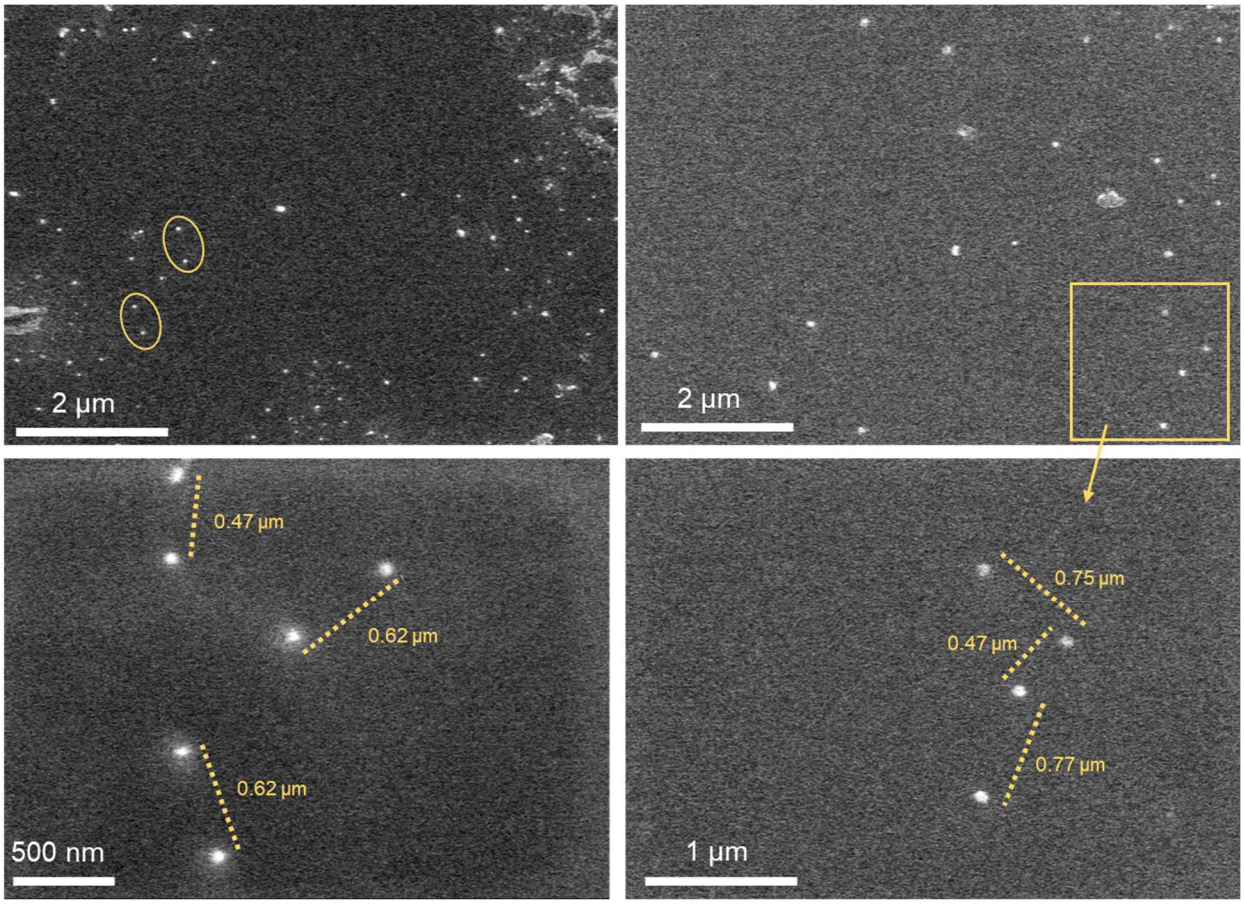

Figure S13: Additional SEM images of SWNT end decorated with sfGFP(G51C)-Car9 and 50 nm Au. (A) Wide field (B) Zoom on several pairs of Au with distances noted (C) Wide field (D) Zoom in of particles from (C) and distances between particles noted

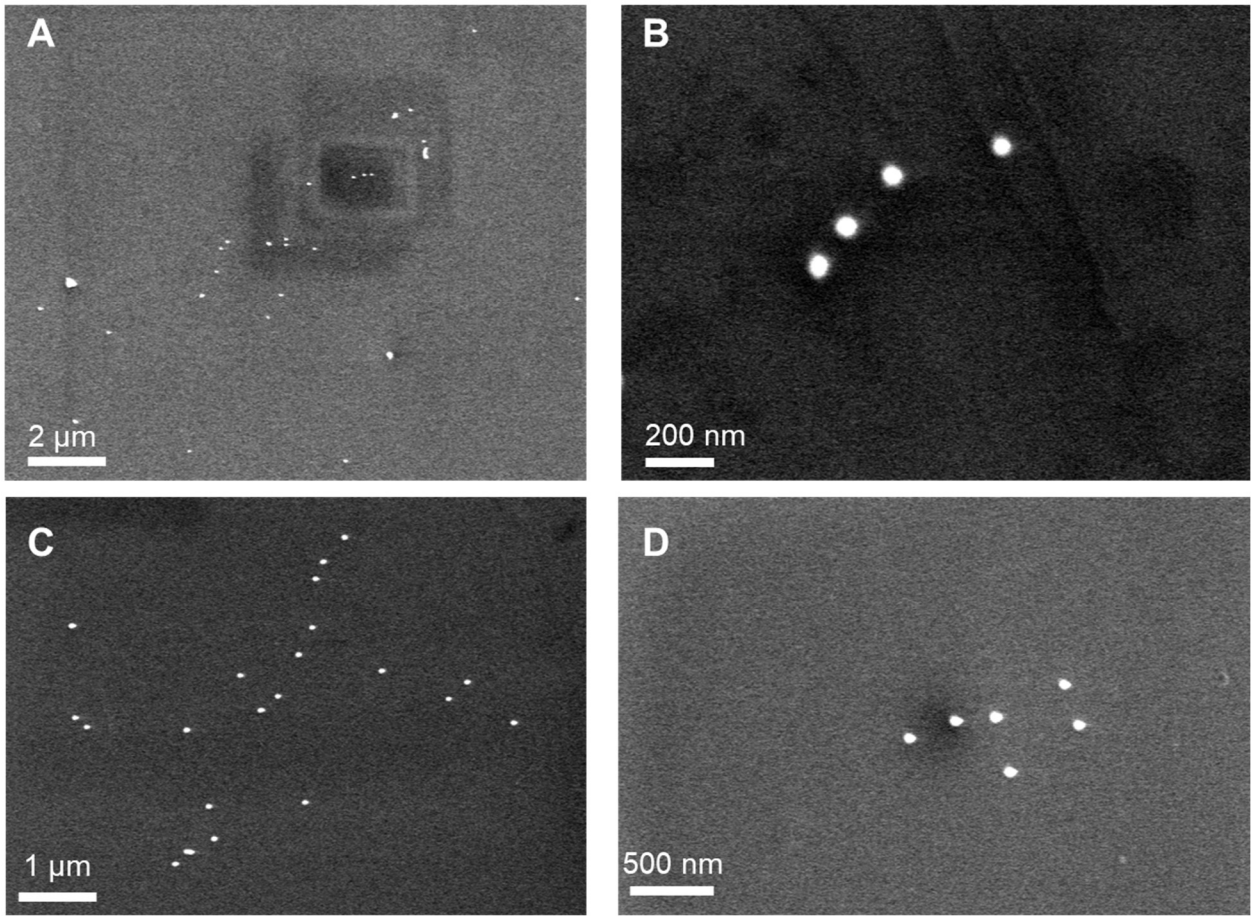

Figure S14: Additional SEM images of SWNT wall decorated with His-sfGFP(G51C)-Car15 and 50 nm Au. (A) Wide field (B) Zoom on several pairs of Au (C) Wide field (D) Zoom on clustering of NP